HIERARCHICAL FINITE ELEMENTS FOR STRESS CONCENTRATION AND STRESS SINGULARITY PROBLEMS

HARVINDER S. SIDHU

HIERARCHICAL FINITE ELEMENTS FOR STRESS CONCENTRATION AND STRESS SINGULARITY PROBLEMS

by

© Harvinder S. Sidhu, B.E.

A thesis submitted to the School of Graduate
Studies in partial fulfilment of the
requirements for the degree of
Master of Engineering

Faculty of Engineering and Applied Science
Memorial University of Newfoundland

August, 1995

St. John's Newfoundland Canada

To my parents

and

Anjana

ABSTRACT

The *p*-version finite element method offers a distinct advantage of savings in computational time and effort in comparison with the conventional, *h*-version finite element method. The *h*-version uses low order elements and convergence studies are done by successive refinements of the mesh that imply analyzing the problem afresh. In contrast, the *p*-version uses a fixed discretization of the domain and higher order elements are successively employed during convergence studies. The computational advantage results from the use of hierarchical shape functions, coarse meshes and faster rates of convergence with decreased number of degrees of freedom. Consequently, the use of hierarchical finite elements can be especially advantageous for stress concentration and stress singularity problems that require very refined meshes in the *h*-version.

The accuracy of hierarchical finite elements is demonstrated with the use of coarse meshes for beam and T-plate weld joint problems. A 2D "enriched hierarchical" finite element is developed for stress intensity factor evaluation that embodies the inverse square root stress singularity by including in its formulation the stress intensity factors as additional degrees of freedom. Stress intensity factors for cracked specimens are numerically evaluated quite accurately using very coarse meshes involving fewer degrees of freedom in comparison with conventional analyses. This concept is then extended to 3D crack problems and favourable results are obtained.

ACKNOWLEDGEMENTS

I would like to express my sincere thanks to Dr. K. Munaswamy, my research supervisor, for his invaluable guidance, encouragement and financial support during the pursuit of my Master of Engineering degree.

I am thankful to Dr. R. Seshadri, Dean, Faculty of Engineering and Applied Science for his continued interest and advice during my graduate program. I gratefully acknowledge the valuable help received from Dr. J.J. Sharp, Associate Dean, Faculty of Engineering and Applied Science for making my stay at Memorial a pleasant one.

I am also grateful to the School of Graduate Studies and the Faculty of Engineering and Applied Science for providing financial assistance without which this work would not have been possible.

Profound thanks to my dear wife Anjana for her love, understanding and constant moral support.

CONTENTS

LIST OF FIGURES

LIST OF TABLES

SYMBOLS AND ABBREVIATIONS

$< >$	Row vector
$\{ \}$	Column vector
$[ ]$	Matrix
N^p	Shape function of order p
G^p	Geometric shape function of order p
$[n]$	Reference number n
K_I, K_{II}, K_{III}	Mode I, Mode II, Mode II stress intensity factors
w.r.t.	with respect to
2D, 3D	Two dimensional, three dimensional
AWS	American Welding Society
CPU	Central Processing Unit
DOF	Degrees of Freedom
EH-	Enriched Hierarchical-
FE	Finite Element
FEM	Finite Element Method
LEFM	Linear Elastic Fracture Mechanics
MUNSID	Finite element analysis program developed
NDOF	Number of DOF
P-	Hierarchical-
RI	Reduced Integration
SCF	Stress Concentration Factor
SIF	Stress Intensity Factor

Chapter I

INTRODUCTION

1.1 Finite Element Method

Finite element method is the most popular and widely used technique for the computational analysis of engineering problems. The procedures involved in the finite element method are : The formulation of the problem in displacement, variational or weighted residual form, the finite element discretization and the effective solution of the resulting system of equations. These basic steps are the same for almost all kinds of problems and the final result is a complete numerical process implemented on the digital computer. The computational time and effort is involved in the following : The formulation and the numerical integration of the finite element matrices, the assemblage of the element matrices into the complete finite element system matrices and the numerical solution of the system equilibrium equations.

Finite elements are employed to represent, depending on the type of problem, beam, truss members, regions of plane stress, plane strain, and axisymmetric, three-dimensional, plate or shell behaviour. A suitable division of the problem domain is

essential to any analysis, in addition, it becomes important for the analyst to refine the mesh of elements in some suitable manner to enhance and determine the accuracy of the analysis through convergence studies. For the analysis of complex problems, where complexity is due to the geometry or stress raisers like stress concentration regions and cracks, a detailed mesh is required. This introduces a large number of unknown variables which increases the computational effort required in the numerical process. The procedure is repeated by remeshing and reanalyzing the problem for convergence studies. Complex systems also involve considerable human effort for design, verification and refinements of the mesh. The overall time and effort required for a computer analysis increases in proportion to the number of unknown variables and complexity of the required mesh. For any analysis it is desirable to reduce both the human and the computer time and effort as these resources are always limited.

Convergence studies, which are essential to any analysis, can be undertaken in two ways. The conventional method is the sub-division of the mesh into a finer mesh, which decreases the size and increases the number of finite elements that represent the domain, especially at areas of stress concentrations and stress singularities. This is called *h-refinement* or simply *mesh refinement*, where *h* refers to the size of the element and the method is referred to as the *h*-version finite element method (FEM). The second uncommon but powerful method is to increase the polynomial order of interpolation functions for the unknown variables associated with the elements, selectively or over the entire domain. This is known as *p-refinement* or simply *mesh enrichment*, where *p* refers to the order of the element and the analysis is said to employ *p*-version FEM.

Convergence is said to be achieved as $h \rightarrow 0$ (h-convergence) or as $p \rightarrow \infty$ (p-convergence).

1.2 p-version FEM

In p-version FEM, p, the order of the element implies the order of the interpolation function for the unknown variable over the elemental domain. *Mesh enrichment* can further be performed in two ways, viz., i) with elements that use regular (non-hierarchical) interpolation functions of higher order, and ii) with elements that use higher order "hierarchical" interpolation functions. Hierarchical implies that the lower order interpolation functions form a subset of the interpolation functions of higher orders. The use of higher order elements with non-hierarchic interpolation functions does not reduce the computational time and effort appreciably as additional data is required for the new unknowns or degrees of freedom and the entire system of higher order matrices needs to be re-computed and re-solved. With the use of hierarchical elements only the matrices that correspond to the "additional" degrees of freedom need to be evaluated and assembled, thus reducing the computational effort. In addition, less effort is required in the solution stage during convergence studies as lower order system matrices form a subset of higher order system matrices. The use of p-version FEM results in fewer degrees of freedom for an analysis due to improved convergence rates that vary in a geometric progression compared with algebraic progression for h-version. In this work, p-version refers to the use of hierarchical finite elements unless otherwise mentioned.

Hierarchical elements thus employ hierarchical basis or interpolation functions for the unknowns. The advantages of reduction in the computational effort and time are due to the following: Construction of coarse meshes sufficient to model the geometry of the problem; lower order matrices need not be re-evaluated, re-assembled and triangularized as they remain unchanged due to the hierarchical nature and form part of the higher order matrices during convergence studies. Also remeshing can be avoided to a large extent during convergence studies by selecting a suitable mesh for the initial analysis and increasing the order of the elements keeping the size fixed. Due to hierarchical forms the resulting matrices have improved conditioning that allows effective iterative solution techniques to be adopted. The *p*-version FEM also offers ease of error estimation which incorporated suitably into the numerical analysis can lead to self adaptive selective mesh enrichment.

Special problems of interest that find immense use of the finite element method are those that involve stress concentrations due to geometry and stress singularities due to cracks, etc. For such problems *h*-version FEM commonly employs a detailed mesh of quadratic serendipity elements introducing a large number of degrees of freedom. The *p*-version FEM can therefore be effectively employed to reduce the required effort significantly. For stress concentration problems, a detailed mesh of standard serendipity elements over the domain and a very detailed mesh in the stress concentration region is replaced by a coarse mesh of hierarchical elements with a slight refinement at the stress concentration region. The convergence of the solution is then achieved simply by, perhaps selective, mesh enrichment. Stress singularity problems however are not so easy to deal with.

1.3 Computational Fracture Mechanics

Common problems of stress singularity behaviour are those containing notches, cracks, sharp changes in the geometry as in an L-shaped domain, etc. Fracture mechanics deals with such problems and its importance in the analysis of structures with cracks has increased manifold over the recent years. In linear elastic stress analysis the stresses and deflections in the crack tip region depend on a single parameter, known as the stress intensity factor (SIF), K. The magnitude of K depends on the structural geometry and the loading system. If K exceeds the fracture toughness of the material crack instability occurs. Thus evaluation of K for any crack configuration is all that is required to assess whether failure will occur or not. In most instances, closed form solutions are not available and K must be determined numerically. Special finite elements that exhibit inverse square root stress singularity at the crack tip improve the accuracy and reduce the need for a high degree of mesh refinement at the crack tip. A lot of effort has gone into the development of special crack tip elements to deal with the singularities in *h*-version FEM. These elements still require a large amount of computational effort and the evaluation of stress intensity factors for complex geometries, especially in three dimensions, is quite cumbersome. The *p*-version FEM can reduce the effort and therefore can be applied effectively to fracture mechanics problems with development of an efficient crack tip element in some suitable fashion.

1.4 Objectives of the Thesis

A lot of research advocating the advantages of *p*-version FEM has been published, however no commercial *p*-version FE software is yet available. For fracture mechanics problems the commonly used elements such as the distorted quadratic serendipity elements require a very detailed mesh especially in the crack tip region and thus are not computationally efficient. Moreover, in the knowledge of the author, no special crack tip element for efficient use in *p*-version FEM is available in literature.

The objective of this work is, thus, to obtain a practical insight into the numerical accuracy of *p*-version finite element method for plane elasticity problems and to develop an efficient hierarchical crack tip element for linear elastic fracture mechanics problems. Due to the attractive features of a 2D hierarchical crack tip element, it is also decided to extend it to a 3D hierarchical crack tip element. An efficient 3D crack tip element is required as real life fracture mechanics problems are essentially three dimensional in nature and involve a large number of degrees of freedom. The reduction of degrees of freedom mainly through the use of coarse meshes is a boon for any 3D analysis where usually even the visual inspection of the mesh is a tremendous task.

In order to achieve the objectives, a finite element analysis program is developed using hierarchical and hierarchical crack tip elements in conjunction with a suitable solution strategy. The elements are first tested for commonly analyzed problems having analytical

results or reference values and then used to solve practical problems. As the *p*-version is known to be computationally advantageous in comparison with the *h*-version FEM, in this work the emphasis is on the performance of the elements in terms of numerical accuracy.

1.5 Layout of the Thesis

Chapter one gives an introduction to the *h*- and *p*-versions of the finite element method. *Chapter two* provides a detailed literature review on the relevant topics and defines the scope of this study. The formulation of the *p*-version finite element method is given in the *chapter three* along with the formulation of the special crack tip element used for fracture mechanics problems for both two-dimensional plane elasticity and three-dimensional problems. The implementation of the formulation is discussed in *chapter four* vis-a-vis the development of a finite element program MUNSID. It also includes a brief discussion of the computational effort for the *p*-version FE program. *Chapter five* presents the numerical results obtained from the analysis of test problems for both 2D and 3D analyses. The conclusions of this study and recommendations are presented in *chapter six*.

Chapter II

BACKGROUND AND SCOPE OF WORK

2.1 Literature Review

The finite element method in general includes three basic concepts. The concept of matrix and linear algebra to provide foundation for a thorough understanding of the finite element procedures. The formulation of the finite element method and the numerical procedures to evaluate the element matrices and the matrices of the complete element assemblage. Lastly, methods of efficient solution of the finite element equilibrium equations. These fundamentals are amply illustrated in the text books by many authors, namely, Zienkiewicz [1], Irons [2], Bathe [3], etc. The following sections present the relevant literature review of the *p*-version FEM and the conventional techniques for evaluation of fracture mechanics parameters.

2.1.1 *p*-version FEM

One of the first works on hierarchical *p*-version FEM is by Peano [4]. New families of

C^0 and C^1 interpolation functions are presented complete up to an arbitrary polynomial degree p. These interpolation functions are formulated for triangular elements in area coordinates. The fundamental characteristics of this family of finite elements is : *the shape functions corresponding to an interpolation of order* p *constitute a subset of the set of shape functions corresponding to an interpolation of order* p+1 *and therefore the stiffness matrix of the element of order* p *is a sub-matrix of the stiffness matrix of the element of order* p+1. The nodal variables corresponding to the constant strain triangle (element of order 1) are the functional values at the vertices. For the linear strain triangle (element of order 2) the additional nodal variables are the second derivatives of the approximating function evaluated along the sides at the mid-side points. The shape functions corresponding to the mid-side nodes of the linear strain triangle vanish at the vertices of the triangle. These hierarchical finite elements are noted as indispensable tools for realizing convergence with respect to increasing polynomial orders due to the hierarchical nature of the resulting stiffness matrix, where the triangularization effort is saved by utilizing the already decomposed lower order matrices. With respect to the problem of using different order elements in the same mesh, the higher order derivatives associated with edges in common with a lower order element are set to zero. Peano proposed the selection of the shape functions as closely orthogonal to one another as possible.

Rossow and Katz [5] presented two dimensional C^0 hierarchic triangular finite elements of arbitrary polynomial order. It is shown that elemental arrays for high polynomial order may be efficiently computed by using hierarchal elements together with

precomputed arrays. For polynomial order $p=1$, the nodal variables are the value of the functional variable at each vertex. For $p \geq 2$, the nodal variables are the ones for p-1 in addition to the pth order tangential derivatives at the mid-sides of the element. For a complete polynomial order p, with $(p+1)(p+2)/2$ coefficients, $(p-1)(p-2)/2$ additional nodal variables are defined for $p \geq 3$. These additional nodal variables are taken as mixed partial derivatives of the function evaluated at the origin. When transformed to the global coordinates, these variables do not equate across inter-element boundaries, hence have no effect external to the element and are called internal nodal variables. In a mixed mesh, higher order elements are demoted to lower order elements along the common edges by equating the common nodal variables and eliminating the higher order variables. Relative efficiency of h- and p-convergence with respect to the computational time is compared and p-convergence is observed both globally and at particular points. The technique of employing hierarchical elements, precomputed arrays, and p-convergence appeared competitive in terms of computational efficiency with the conventional finite element approach. Also, the use of large elements simplified the presentation of input data and interpretation of results.

Babuska, Szabo and Katz [6] discuss concepts of p-convergence of the finite element method, the singularity problem, numerical examples and computer implementation of the p-version. The shape functions chosen for a one dimensional bar problem are the integrals of the Legendre's polynomials which form an orthogonal family with respect to the energy inner product. For the computer implementation precomputed arrays based on hierarchic families are utilized. It is noted that as the number of degrees of freedom

increase progressively, major computational effort occurs in the solution phase. For the asymptotic rate of convergence with respect to the NDOF: for *smooth solutions*, *p*-convergence is not limited by an upper bound polynomial degree as in *h*-version; and in case of *non-smooth solutions*, when a singularity is caused by corners, the rate of *p*-convergence is almost twice that of *h*-convergence. As *p*-version can be used in conjunction with optimally designed meshes, the mesh design seemed much less critical for the *p*-version than for the *h*-version. Observations include: Reduction in volume of input data; less critical nature of roundoff problems in *p*-version; no major difference in the solution times for *p*-version and *h*-version for the same NDOF; and adaptivity in *p*-version seems simpler by proposing mesh grading on a prior basis, either manually or with standard mesh generators, and then making adaptive changes by adjusting *p*.

Zienkiewicz, Gago and Kelly [7] discuss the merits of hierarchical forms in utilizing previous solutions and computation as well as permitting a simple iteration when attempting a refinement. The hierarchical degrees of freedom appear as perturbations on the original solution rather than its substitute and the resulting matrices have a more dominantly diagonal form than that obtainable from identical number of non-hierarchic degrees of freedom. This ensures an improved conditioning of the matrix and a faster rate of iteration convergence than would be possible with non-hierarchic forms. The perturbation nature of hierarchic forms also provides an immediate estimate of the error in the solution. The paper discusses the error estimates and addresses the issue of adaptive refinement. It is recommended to limit the order p to a maximum of 4 and start from a reasonable mesh not calling for $p>4$, since the use of very high polynomial

orders could lead to local oscillation.

Szabo [8] presents general guidelines for prior design of meshes. It is noted that with the use of properly designed meshes, the performance of *p*-enrichment is very close to the best performance attainable by the finite element method. The estimation and control of the error in finite element analysis are based on *h*- or *p*-refinements and *p*-refinement makes it convenient and inexpensive to obtain information about the quality of the finite element solutions. The proposed mesh design is the coarsest possible mesh controlled entirely by the geometry of the domain when the exact solution is smooth. The only restriction on the mesh is the smooth mapping of the elements. In case of non-smooth exact solutions, the points of singularity and areas of stress concentration need to be isolated by one or more layers of small elements and the mesh is graded such that the element sizes are in geometric progression with the smallest element(s) located where the stress gradients are the largest. The geometric progression with a common factor of about 0.15 is found suitable. In the case of structures with many singularities it is found not necessary to refine the mesh in the neighbourhood of every singular point with care being taken that overall and local equilibrium conditions are satisfied. Babuska [9] also gives reference to optimal design of meshes.

Wieberg and Moller [10] describe hierarchical FE-formulation and adaptive procedures for static and dynamic problems. The sequence of nested equation systems that results from a hierarchical finite element formulation is examined. Due to the special structure of the matrices formulated using hierarchic basis functions and ease of developing error

indicators for further refinements, iterative solution procedures are used when an increasing number of variables are introduced into the approximations. New possibilities are presented for iterative solution of nested equation systems for elastic static problems resulting from hierarchic basis functions. Out of the four algorithms outlined, three are based on the pre-conditioned conjugate gradient method and the fourth is a two-level multigrid method.

Babuska, Griebel and Pitkaranta [11] address the question of optimal selection of the shape functions for *p*-type finite elements and discusses the effectiveness of the conjugate gradient and multilevel iteration method for solving the corresponding linear system. A unit square master element is considered and the three groups of shape functions associated with the element are, namely, the nodal shape functions, the side shape functions and the internal shape functions. A nodal shape function is associated with a vertex of the element and is zero on the opposite sides of the vertex it is associated with. A side shape function is associated with a side and is zero on all three other sides of the element. An internal shape function is zero on all four sides and has the character of a 'bubble' function. Various sets of these shape functions are considered along with the non-hierarchic shape functions and trigonometric shape functions. These sets are then compared for optimal selection of shape functions through computational analysis. Only two dimensional cases are addressed in the paper.

Morris, Tsuji and Carnevali [12] proposed and implemented a solution strategy for taking advantage of the hierarchical structure of linear equation sets. The key novelty of the

algorithm is the ability to choose dynamically between iterative and direct solution techniques based on a set of heuristics. The iterative solver is based on the conjugate gradient method and the combination of the direct and iterative solvers allow for an efficient solution path, having the robustness of a direct solution algorithm, and the efficiency of an iterative solver in utilization of both CPU and storage.

A valuable discussion on the state of the art of the *p*-version of the finite element method is given in Babuska [9]. Various theorems are presented to define the *p*- and *hp*-version of the FEM. A numerical example illustrates the performance of *p*-version with different number of layers at the stress singularity point (graded mesh) and compares it to a uniform mesh. For implementation the three kinds of shape functions discussed are nodal, side and internal shape functions. For the computation of the local stiffness matrix the rule for number of Gauss points is $2[integer(p/2)] + 2$. The *p*- and *hp*-versions for two-dimensional problems were implemented in the commercial software PROBE by Noetic Tech., St. Louis with the first release in 1985 and the second in 1986 and it was tested and used extensively in the industry. The features considered important by the engineering users were increased level of confidence in the computation, lower human time requirement due to simplicity and flexibility of input, rapid convergence and flexibility including the use of large aspect ratios, flexibility of mesh design, easy learning and robust performance.

2.1.2 Computational fracture mechanics

Chan, Tuba and Wilson [13] used the finite element method for the evaluation of stress intensity factors. The displacement FEM is used and first order displacement functions for triangular elements are assumed, in which, the displacements vary linearly over the element resulting in constant strains and stresses in the element. A very detailed mesh is considered where the smallest elements are difficult to see with the naked eye. For the computation of stress intensity factors, three approaches outlined are the displacement method, stress method and the line integral (energy) method. The stress intensity factors in the displacement method are determined from the correlation of the finite element nodal point displacements with the well known crack tip displacement equations. The stress method is similar to the displacement method and the nodal point stresses are correlated with the known crack tip stress equations. In the line integral method, the line integral J given by Rice [14] is numerically integrated along an arbitrary contour surrounding the crack tip and the stress intensity factor is evaluated as a function of J, modulus of elasticity and the Poisson's ratio. The elements however do not represent the singular near tip deformation and the analyses included a very large number of degrees of freedom. They proposed potential improvements by including higher order displacement functions.

Tracey [15] introduced a new type of two-dimensional finite element which incorporates the inverse square root singularity in stresses near a crack tip in an elastic medium. Triangular "singular" elements that are proposed embody the singular stress fields corresponding to the crack tip. The crack tip serves as the centre of a whole ring of

triangular elements and joined in the radial direction with quadrilateral isoparametric elements of order one. These triangular elements are four node quadrilaterals with two nodes coincident at the crack tip but distinguishable by their angular rotation. Tracey [16] also described a special three-dimensional element analogous to the two-dimensional element for evaluation of stress intensity factors. In this formulation a six node wedge shaped singularity element with special displacement interpolation functions is focussed around the crack front and is surrounded by eight noded isoparametric brick elements. An eight point Gaussian quadrature is used to evaluate the stiffness matrix.

Hellen [17] proposed a virtual crack extension method where the energy release rates are computed using virtual crack extensions. The stress intensity factors are evaluated using their known relationship with energy release rate for a virtual amount of crack growth. An algorithm is devised to calculate the energy difference for two crack positions, close together, using only one mesh, and altering the tip stiffnesses to assess the energy difference. To increase the accuracy of results, quadratic special crack tip elements developed by Blackburn [20] are used in conjunction with the proposed method. The special elements are triangular in two dimensions with $r^{1/2}$ displacement variation radiating from the crack tip, where r is the radial distance from the crack tip.

Henshell and Shaw [18] introduced the required singularity at the corner of a quadrilateral isoparametric finite element by moving the mid-side nodes to the quarter point towards the crack tip. For determination of stress intensity factors in cracked bodies it is suggested to use the standard quadratic isoparametric elements with the

distorted isoparametric elements at the crack tip. However the results obtained by displacement methods depended on the point chosen for displacement evaluation and reliable results were obtained by using displacements at points along the free surface of the crack.

Barsoum [19] individually developed singular elements based on the same technique used by Henshell and Shaw [18] for the evaluation of stress intensity factors. Eight noded quadrilateral, six-noded triangular elements and three dimensional twenty noded cubic and prism elements are distorted by moving mid-side nodes closest to the crack at the quarter points. This results in a $r^{-1/2}$ stress singularity at the crack tip corresponding to the theoretical stress singularity of linear fracture mechanics. The elements are shown to have rigid body motion and constant strain modes and satisfy the patch test. In both cases [18,19] a sizeable number of elements are required to model the crack tip as well as the rest of the problem domain.

Blackburn [20] presented a triangular element with vertex and mid-edge nodes with special displacement functions to represent the singularity behaviour in two-dimensional problems. Blackburn and Hellen [21] extended the special two-dimensional element to three-dimensional problems as a 15 noded wedge shaped special crack tip element. The stress intensity factors are calculated by displacement method, line integral method and also by the method of virtual crack extensions.

Benzley [22] developed a special crack tip element from a linear isoparametric element,

with one corner corresponding to the crack tip, and enriching the conventional displacement assumption with the displacement field corresponding to the singular portion of the elasticity solution. In addition to nodal displacements, K_I and K_{II} become basic unknowns in such elements and are calculated directly in the finite element analysis. A linear zeroing function is used for the enriched elements to make them compatible with the adjacent non-enriched elements.

Gifford and Hilton [23] enriched a conventional quadratic isoparametric element as suggested by Benzley. However the element formulation is of the non-conforming type and no zeroing function is considered. 8x8 numerical quadrature is required for the accurate numerical integration of the enriched element.

Raju and Newman [24] presented stress intensity factors for shallow and deep semi-elliptical surface cracks in plates subjected to uniform tension. The stress intensity factors are evaluated using nodal force method and the finite element models constructed using singular and isoparametric elements involve a very large number of degrees of freedom. The results presented in this paper are widely used for reference as well as for comparison studies.

Heppler and Hansen [25] utilized Gifford and Hilton's twelve node enriched serendipity element for the calculation of linear elastic planar stress intensity factors for rectilinear anisotropic materials subjected to biaxial loading. In addition, conforming formulations using three different zeroing functions, linear, super-ellipse and polynomial, are studied

and compared with non-conforming formulations. For the non-conforming case high accuracy is achieved with a few elements and they noted a substantial stiffening of the finite element model for the conforming cases. Among the three zeroing functions, the polynomial function which reinforces the expected singular behaviour near the crack tip performed the best.

2.2 Scope of the Study

A static p-version finite element analysis program that employs quadrilateral hierarchical finite elements is developed for plane elasticity problems. The interpolation functions for P-elements are enriched to derive special crack tip elements (enriched hierarchical elements) for use in linear elastic fracture mechanics problems. All analyses study p-convergence thereby eliminating the need for redesign of mesh for convergence studies.

2.2.1 Formulation of 2D-hierarchical element

The shape functions for quadrilateral hierarchical elements are derived from Legendre's polynomials. The interpolation functions are incomplete polynomials in a fashion similar to that of standard serendipity elements. For an element of order p there are $4p$ nodes each having two degrees of freedom. The nodal variables corresponding to the corner nodes are the physical degrees of freedom, the displacements u and v, in the global cartesian coordinates, x and y respectively. The higher order nodal variables for the pth order element are the pth derivatives of the displacements along the side at the mid-side

node. For evaluation of the stiffness matrices, $p+1$ gauss quadrature is adopted for an element of order p.

2.2.2 Formulation of 2D-enriched hierarchical element

The enrichment of the hierarchical element is based on Benzley's [22] principle due to simplicity of the formulation and as the stress intensity factors are presented directly in the output. For the compatibility of adjacent P- and EH-elements a zeroing function is required for the EH-element, however it has been shown in [25] that the zeroing function stiffens the system. Therefore no zeroing function for the EH-element is considered, the formulation is a non-conforming one and is similar to that used by Gifford and Hilton [23] for a serendipity element. The crack element stiffness matrices are numerically integrated by using 8 point gauss quadrature.

2.2.3 Formulation of 3D P- and EH-elements

The shape functions used for the P-element and the principle for enrichment to the crack tip element for a two-dimensional case are simply extended to three-dimensions.

2.2.4 Solution strategy

The elemental stiffness matrices are assembled into the global stiffness matrix in a skyline format. The global stiffness matrix for high order elements is partitioned, the block diagonal matrices are triangularized by gaussian elimination and a combination of direct and iterative techniques is used for the solution.

2.2.5 Numerical verification and results

The test problems selected for verification of 2D P-element are the commonly used short cantilever beam problem and the Cook's membrane problem. The tests for 2D EH-elements are a double edge cracked tensile specimen and a slant cracked tensile specimen with mixed mode SIF solution.

The practical problem selected is a T-plate weld joint analyzed by Bell [26] for stress concentration and stress intensity factors. The SCF's are evaluated for 45° and AWS weld profiles and the fatigue life of a 45° weld joint is also estimated. The results are then compared with those obtained by Bell.

The test problems for the 3D EH-elements are double edge cracked tensile and compact tension specimens. The double edge crack tensile specimen is an extension of the 2D problem and the selected compact tension specimen is that solved by Tracey [16]. A semi-circular surface crack in a plate subjected to tension is then analyzed and results are compared with those given by Raju and Newman [24].

Chapter III

FINITE ELEMENT FORMULATION

3.1 Generalized FE Formulation

The displacement finite element approach used in this study is derived from the principles of virtual work. This formulation can also be derived using the variational principle or Galerkin's weighted residual approach. For two dimensional plane elasticity problems the unknowns are the displacements u and v in the global X and Y coordinate system. The displacements are first interpolated over the domain of an element represented by a local coordinate system. The standard procedures given in [1,2,3] are then used to determine the shape functions. The quadrilateral master element in local ξ and η coordinate system is represented in Fig. 3.1. The values of local coordinates for the element lie between ± 1. The interpolation of

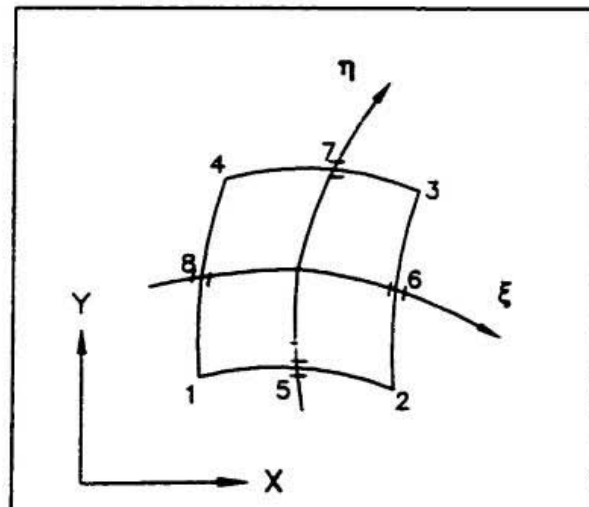

Figure 3.1 Quadrilateral master element

displacements u and v in terms of nodal variables, by appropriate shape functions N, in any region of the local element is given by :

$$u^e = \langle N(\xi,\eta)\rangle\{u^e\}$$
$$v^e = \langle N(\xi,\eta)\rangle\{v^e\} \qquad \ldots (3.1)$$

where $\{u^e\}$ and $\{v^e\}$ are the nodal values for the local element. The strains in the element are given by :

$$\{\varepsilon^e\} = \begin{Bmatrix} \varepsilon_x \\ \varepsilon_y \\ \gamma_{xy} \end{Bmatrix} = \begin{Bmatrix} \dfrac{\partial u}{\partial x} \\ \dfrac{\partial v}{\partial y} \\ \dfrac{\partial u}{\partial y} + \dfrac{\partial v}{\partial x} \end{Bmatrix} = [B]\{d^e\} \qquad \ldots (3.2)$$

where [B] is a matrix containing derivatives of shape functions in the global coordinates and $\{d^e\}$ is the nodal displacement vector given by :

$$\{d^e\} = \langle u_1\ v_1\ \ldots\ u_3\ v_3\ \ldots u_{4p}\ v_{4p}\rangle^T \qquad \ldots (3.3)$$

u_1 denotes u at node 1, and p is the order of the interpolation function.

The mapping of the local element to the global element required for the evaluation of global stresses and strains is done by the Jacobian J, that depends on the geometry of the global element. The geometry of the element is approximated in terms of the nodal coordinates (x_i,y_i) by suitable geometric shape functions, G :

$$x = \sum_{i=1}^{4p} G_i \, x_i$$

$$y = \sum_{i=1}^{4p} G_i \, y_i \qquad \text{. . (3.4)}$$

The formulation is sub-, iso- or super-parametric if the order of G (given as p in Eqn.(3.4)) is less than, equal to or greater than the order of N respectively. The Jacobian J is given by :

$$[J] = \begin{bmatrix} \frac{\partial x}{\partial \xi} & \frac{\partial y}{\partial \xi} \\ \frac{\partial x}{\partial \eta} & \frac{\partial y}{\partial \eta} \end{bmatrix} \qquad \text{. . (3.5)}$$

Using Eqn.(3.4) we have :

$$[J] = \begin{bmatrix} \frac{\partial \langle G \rangle}{\partial \xi} \\ \frac{\partial \langle G \rangle}{\partial \eta} \end{bmatrix} [\{x\}\{y\}] \qquad \text{. . (3.6)}$$

The [B] matrix is partitioned into sub-matrices corresponding to each node, and is given by :

$$[B] = \langle \, . \, . \, . | B_i | \, . \, . \, . \rangle$$

$$[B_i] = \begin{bmatrix} \frac{\partial N_i}{\partial x} & 0 \\ 0 & \frac{\partial N_i}{\partial y} \\ \frac{\partial N_i}{\partial y} & \frac{\partial N_i}{\partial x} \end{bmatrix} \qquad \text{. . (3.7)}$$

where the sub-matrix $[B_i]$ corresponds to the ith node. Since the displacement shape functions are formulated in local coordinates, to determine the elements of matrix $[B_i]$, the following relationship is used :

$$\begin{Bmatrix} \frac{\partial N_i}{\partial x} \\ \frac{\partial N_i}{\partial y} \end{Bmatrix} = [J]^{-1} \begin{Bmatrix} \frac{\partial N_i}{\partial \xi} \\ \frac{\partial N_i}{\partial \eta} \end{Bmatrix} \qquad \ldots (3.8)$$

The elemental stresses are obtained by the constitutive law :

$$\{\sigma^e\} = \begin{Bmatrix} \sigma_x \\ \sigma_y \\ \tau_{xy} \end{Bmatrix} = [D]\{\varepsilon^e\} = [D][B]\{d^e\} \qquad \ldots (3.9)$$

where [D], the constitutive matrix given for plane strain ($p\varepsilon$) is :

$$[D]_{p\varepsilon} = \frac{E}{(1+\nu)(1-2\nu)} \begin{bmatrix} 1-\nu & \nu & 0 \\ \nu & 1-\nu & 0 \\ 0 & 0 & \frac{1-2\nu}{2} \end{bmatrix} \qquad \ldots (3.10)$$

and for plane stress ($p\sigma$) is :

$$[D]_{p\sigma} = \frac{E}{1-\nu^2} \begin{bmatrix} 1 & \nu & 0 \\ \nu & 1 & 0 \\ 0 & 0 & \frac{1-\nu}{2} \end{bmatrix} \qquad \ldots (3.11)$$

The stiffness matrix and the load vector (considering only surface forces) for an element are given by :

$$[K^e] = \int_{\Omega} [B]^T [D] [B] \, d\Omega$$

$$[F^e] = \int_{\Gamma} \langle N \rangle^T f_s \, d\Gamma \qquad \text{. . (3.12)}$$

where Ω represents the domain of the element and a surface load f_s acts on the boundary Γ. The stiffness matrix is formulated in the local coordinate system hence it is written as :

$$[K^e] = \int_{-1}^{1} \int_{-1}^{1} [B]^T [D] [B] \, d\xi \, d\eta \, |J| \qquad \text{. . (3.13)}$$

where $|J|$ is the determinant of the Jacobian. Gauss quadrature rule is applied to numerically integrate the element stiffness matrix given in Eqn.(3.13). Gauss integration using NGxNG points is given as :

$$[K^e] = \sum_{i=1}^{NG} \sum_{j=1}^{NG} [B(\xi_i,\eta_j)]^T [D] [B(\xi_i,\eta_j)] \, |J(\xi_i,\eta_j)| \, w_i \, w_j \qquad \text{. . (3.14)}$$

w_i and w_j are the weights corresponding to *i*th and *j*th gauss points respectively.

Once the stiffness matrices of all the elements representing the domain are evaluated as described above, the global stiffness and load matrices are obtained by the summation or assembly of the elements of local matrices to the corresponding elements of global matrices :

$$[K^G] = \sum_{e} [K^e]$$

$$[F^G] = \sum_{e} [F^e] \qquad \text{. . (3.15)}$$

The system of equations in the displacement formulation of the FEM is given as :

$$[K^G]\{d\} = \{F^G\} \qquad \ldots (3.16)$$

where {d} is the global vector of nodal displacements.

The displacement shape functions, N, in *p*-version FEM are hierarchical in nature and are discussed in the next section. The geometric shape functions, G^p, are chosen as the linear and quadratic serendipity shape functions corresponding to a quadrilateral master element for order (*p*) one and two respectively :

$$G_i^1 = \frac{1}{4}(1+\xi\xi_i)(1+\eta\eta_i) \qquad i = 1,2,3,4$$

$$\begin{aligned} G_i^2 &= \frac{1}{4}(1+\xi\xi_i)(1+\eta\eta_i)(\xi\xi_i+\eta\eta_i-1), && i = 1,2,3,4 \\ &= \frac{1}{2}(1-\xi^2)(1+\eta\eta_i), && i = 5,7 \\ &= \frac{1}{2}(1+\xi\xi_i)(1-\eta^2), && i = 6,8 \end{aligned} \qquad \ldots (3.17)$$

The geometric shape functions given in Eqn.(3.17) are also used as displacement shape functions for *h*-type elements in the *h*-version FEM and are an entirely different set for different orders.

3.2 *p*-version FE Formulation

This section presents the hierarchical shape functions used in this work. For the illustration purposes the derivation for a second order hierarchical element is discussed

in particular. In addition only the derivations for displacement u are provided and are obtained for v in an analogous manner.

The displacement interpolation for u over the local quadrilateral element is given by :

$$\begin{aligned} u^e &= \alpha_0 + \alpha_1\xi + \alpha_2\eta + \alpha_3\xi\eta + \alpha_4\xi^2 + \alpha_5\eta^2 + \alpha_6\xi^2\eta + \alpha_7\xi\eta^2 \\ &= \langle P\rangle\{\alpha\} \end{aligned} \quad \ldots (3.18)$$

where $\{\alpha\}$ is the coefficient vector. The nodes corresponding to a hierarchical element are the four corner nodes for the first order and for each increment in order a set of four hierarchical nodes is placed, one at each of the four mid-sides. Thus, for a second order P-element there are four corner nodes and four hierarchical mid-side nodes. Evaluating u in Eqn.(3.18) at the four corner nodes we have :

$$\begin{aligned} u_1^e &= \alpha_0 - \alpha_1 - \alpha_2 + \alpha_3 + \alpha_4 + \alpha_5 - \alpha_6 - \alpha_7 \\ &\vdots \\ u_4^e &= \alpha_0 - \alpha_1 + \alpha_2 - \alpha_3 + \alpha_4 + \alpha_5 + \alpha_6 - \alpha_7 \end{aligned} \quad \ldots (3.19)$$

The degree of freedom at the mid-side node is the hierarchical degree of freedom defined as the double derivative of the displacement along the side on which the node lies, and is evaluated at that node. Thus this pseudo "displacement" at the mid-side node 5 is given by :

$$u_5^e = \left[\frac{d^2}{ds^2}\{u^e(\xi,-1)\}\right]_5 = \left[\frac{d^2}{d\xi^2}\{u^e(\xi,-1)\}\right]_5 \left(\frac{2}{l_5}\right)^2 = (\alpha_4 - \alpha_6)\left(\frac{2}{l_5}\right)^2 \quad \ldots (3.20)$$

where l_5 is the length of the side on which node 5 lies. Similarly the hierarchical

variables at the nodes 6, 7 and 8 are evaluated. The coefficient matrix $\{\alpha\}$ is obtained in terms of the nodal variables and is used in Eqn.(3.18) to obtain the displacements in terms of nodal variables via shape functions. The operation is given as :

$$\{u^e\} = [C]\{\alpha\}$$

$$\{\alpha\} = [C]^{-1}\{u^e\} \qquad \text{. . (3.21)}$$

$$u^e = [P][C]^{-1}\{u^e\} = \langle N\rangle\{u^e\}$$

The shape functions N obtained in this fashion are hierarchical in nature. The hierarchical shape functions however are not unique. The first order P-shape functions correspond to the corner nodes and are equal to the first order serendipity shape functions, G^i, given in Eqn.(3.17). To reduce coupling between successive solutions the higher order shape functions are derived from Legendre's polynomials that are orthogonal in the -1 to +1 range. A one dimensional polynomial term, L^p, for the pth order shape function for a line element corresponding to a side of the master element having two corner nodes and one mid-side node is obtained as :

$$L^{p-1} = \int P_p(\xi)\, d\xi = \frac{1}{(p-1)!\ 2^{p-1}} \frac{d^{p-1}}{d\xi^{p-1}}[(\xi^2-1)^p] \qquad \text{. . (3.22)}$$

where P_p is the Legendre's polynomial of order p. The polynomial expression for the second order, L^2, is :

$$L^2 = (\xi^2-1) \qquad \text{. . (3.23)}$$

and polynomial expression for the shape function for the mid-side node 5 (along $\eta=-1$) is obtained as :

$$N_5^2 = L^2(1-\eta) \qquad \text{. . (3.24)}$$

For the second order hierarchical variable the double derivative of this shape function, Eqn.(3.24) must equal unity at node 5. Thus

$$\left(\frac{\partial^2}{\partial s^2}[N_5^2]\right)_5 = 1 \qquad \text{. . (3.25)}$$

and the complete set of 2nd order hierarchical shape functions for a quadratic P-element corresponding to the four mid-side nodes is :

$$\begin{aligned} N_i^p = N_5^2 &= \frac{1}{4}(\xi^2-1)(1-\eta)\left(\frac{l_5}{2}\right)^2 \\ N_6^2 &= \frac{1}{4}(1+\xi)(\eta^2-1)\left(\frac{l_6}{2}\right)^2 \\ N_7^2 &= \frac{1}{4}(\xi^2-1)(1+\eta)\left(\frac{l_7}{2}\right)^2 \\ N_8^2 &= \frac{1}{4}(1-\xi)(\eta^2-1)\left(\frac{l_8}{2}\right)^2 \end{aligned} \qquad \text{. . (3.26)}$$

For a third order element out of a total of twelve shape functions, the four corner shape functions remain the same i.e. equal to G^1, and four mid-side shape functions are the same as given in Eqn.(3.26). The remaining four additional shape functions correspond to the new hierarchical degrees of freedom (the third derivative of the displacement along the side) and are similarly derived. In this study only nodal and side shape functions are considered thus an element of order p has $4p$ nodes (4 corner and $4p$-4 mid-side) and $4p$

corresponding shape functions.

3.3 2D EH-Element

For a body containing a crack the local coordinate system at the crack tip is illustrated in Fig. 3.2. x' and y' are the local axes centred at the crack tip with x' axis oriented along the crack plane. r and Θ are the polar coordinates of a point in the crack tip region w.r.t. the local x', y' axes. ϕ is the orientation of the crack tip w.r.t. the global X axis, measured +ve counter-clockwise. The displacements in the vicinity of the crack tip given by Gifford and Hilton [23] are :

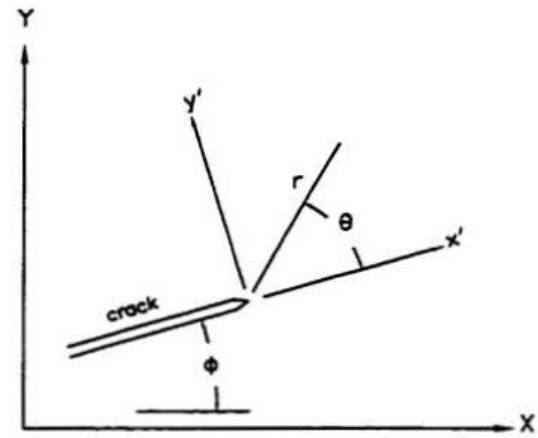

Figure 3.2 Coordinate system at crack tip

$$u_c = K_I f_1 + K_{II} g_1$$
$$v_c = K_I f_2 + K_{II} g_2 \qquad \text{. . (3.27)}$$

where f_1, g_1, etc. are functions that depend on r, Θ and ϕ in the crack tip coordinate system, G the shear modulus and ν the Poisson's ratio. K_I and K_{II} are the mode I (tension) and mode II (shear) stress intensity factors. The functions f_1, etc. are given as :

$$f_1 = \frac{1}{4G}\sqrt{\left(\frac{r}{2\pi}\right)}\{\cos\phi\ [(2\gamma-1)\cos\frac{\theta}{2} - \cos\frac{3\theta}{2}]$$
$$- \sin\phi\ [(2\gamma+1)\sin\frac{\theta}{2} - \sin\frac{3\theta}{2}]\} \quad \ldots (3.28)$$
$$g_1 = \frac{1}{4G}\sqrt{\left(\frac{r}{2\pi}\right)}\{\cos\phi\ [(2\gamma+3)\sin\frac{\theta}{2} + \sin\frac{3\theta}{2}]$$
$$+ \sin\phi\ [(2\gamma-3)\cos\frac{\theta}{2} + \cos\frac{3\theta}{2}]\}$$

$$f_2 = \frac{1}{4G}\sqrt{\left(\frac{r}{2\pi}\right)}\{\sin\phi\ [(2\gamma-1)\cos\frac{\theta}{2} - \cos\frac{3\theta}{2}]$$
$$+ \cos\phi\ [(2\gamma+1)\sin\frac{\theta}{2} - \sin\frac{3\theta}{2}]\} \quad \ldots (3.29)$$
$$g_2 = \frac{1}{4G}\sqrt{\left(\frac{r}{2\pi}\right)}\{\sin\phi\ [(2\gamma+3)\sin\frac{\theta}{2} + \sin\frac{3\theta}{2}]$$
$$- \cos\phi\ [(2\gamma-3)\cos\frac{\theta}{2} + \cos\frac{3\theta}{2}]\}$$

where

$$\gamma = \begin{cases} 3-4\nu & \text{plane strain} \\ \dfrac{3-\nu}{1+\nu} & \text{plane stress} \end{cases} \quad \ldots (3.30)$$

The hierarchical element displacement assumption, Eqn.(3.18), is enriched by the crack tip displacement as :

$$u^e_{EH} = u^e + u_c \quad \ldots (3.31)$$
$$= [P]\{\alpha\} + K_I f_1 + K_{II} g_1$$

Proceeding in a standard sequence, Eqn.(3.18) to Eqn.(3.21), for evaluating the

displacements in an element in terms of the nodal variables, the displacement interpolation of the "enriched" second order P-element is given by :

$$u^e_{EH} = \langle N \rangle \{u^e\} + K_I \left[f_1 - \sum_{i=1}^{4} N_i \, f_{1i} - \sum_{i=5}^{8} N_i \, f''_{1i} \right] + K_{II} \left[g_1 - \sum_{i=1}^{4} N_i \, g_{1i} - \sum_{i=5}^{8} N_i \, g''_{1i} \right] \quad \text{. . (3.32)}$$

$$= \langle N \rangle \{u^e\} + K_I \, P_1 + K_{II} \, Q_1$$

$$v^e_{EH} = \langle N \rangle \{v^e\} + K_I \left[f_2 - \sum_{i=1}^{4} N_i \, f_{2i} - \sum_{i=5}^{8} N_i \, f''_{2i} \right] + K_{II} \left[g_2 - \sum_{i=1}^{4} N_i \, g_{2i} - \sum_{i=5}^{8} N_i \, g''_{2i} \right] \quad \text{. . (3.33)}$$

$$= \langle N \rangle \{v^e\} + K_I \, P_2 + K_{II} \, Q_2$$

f''_{1i} is similar to the definition of hierarchic nodal variables and is given by :

$$f''_{1i} = \left. \frac{\partial^2 (f_1)}{\partial s^2} \right|_i \quad \text{. . (3.34)}$$

and is evaluated at the *i*th node. The displacement interpolation u for an enriched hierarchical element of arbitrary order p is given by :

$$u^e_{EH} = \langle N \rangle \{u^e\} + K_I \left[f_1 - \sum_{i=1}^{4} N_i \, f_{1i} - \sum_{p=2}^{P} \sum_{j=1}^{4} N_j^p \, f'^p_{1j} \right] + K_{II} \left[g_1 - \sum_{i=1}^{4} N_i \, g_{1i} - \sum_{p=2}^{P} \sum_{j=1}^{4} N_j^p \, g'^p_{1j} \right] \quad \text{. . (3.35)}$$

where i and j correspond to the corner and mid-side nodes respectively.

The strains in a second order P-element are given by :

$$\varepsilon_x^e = \frac{\partial \langle N \rangle}{\partial x}\{u^e\} + K_I \frac{\partial P_1}{\partial x} + K_{II} \frac{\partial Q_1}{\partial x}$$

$$\varepsilon_y^e = \frac{\partial \langle N \rangle}{\partial y}\{v^e\} + K_I \frac{\partial P_2}{\partial y} + K_{II} \frac{\partial Q_2}{\partial y} \qquad \text{. . (3.36)}$$

$$\gamma_{xy}^e = \left(\frac{\partial \langle N \rangle}{\partial x}\{v^e\} + \frac{\partial \langle N \rangle}{\partial y}\{u^e\}\right) + K_I \left(\frac{\partial P_1}{\partial y} + \frac{\partial P_2}{\partial x}\right) + K_{II} \left(\frac{\partial Q_1}{\partial y} + \frac{\partial Q_2}{\partial x}\right)$$

which in matrix form are :

$$\{\varepsilon^e\} = [B_{EH}]\{d_{EH}^e\}$$

$$\{d_{EH}^e\}^T = \langle u_1\ v_1\ u_2\ v_2\ \ldots u_8\ v_8\ K_I\ K_{II} \rangle \qquad \text{. . (3.37)}$$

In this formulation K_I and K_{II} are included as additional degrees of freedom and the corner node corresponding to local coordinates of $\xi = -1$ and $\eta = -1$ is located at the crack tip. For the evaluation of functions f_1, etc., the value of ϕ for the nodes lying on one surface of the crack face is $+180°$ while for the node on the other surface the value is $-180°$. The [B] matrix is partitioned and given as :

$$[B] = \langle B_1 \ldots B_i \ldots B_8\ B_k \rangle$$

$$[B_k] = \begin{bmatrix} \frac{\partial P_1}{\partial x} & \frac{\partial Q_1}{\partial x} \\ \frac{\partial P_2}{\partial y} & \frac{\partial Q_2}{\partial y} \\ \frac{\partial P_1}{\partial y} + \frac{\partial P_2}{\partial x} & \frac{\partial Q_1}{\partial y} + \frac{\partial Q_2}{\partial x} \end{bmatrix} \qquad \text{. . (3.38)}$$

where $[B_i]$ is given in Eqn.(3.7) and $[B_k]$ corresponds to the degrees of freedom (K_I, K_{II}) of the "pseudo" node at the crack tip. The evaluation of the local and global stiffness matrix is the same as described in section 3.2.

3.4 3D P- & EH-Elements

The development of the 3D hierarchic element is a simple extension of the 2D P-element. The master element is defined in the local ξ, η, ζ coordinates as shown in Fig. 3.3. The displacement shape functions for a 2nd order 3D hierarchic element are given in appendix A. The geometric shape functions, G, for order 1 and 2 are the serendipity shape functions associated with an 8-noded and a 20-noded serendipity brick element respectively. The Jacobian for the 3D P-element is given by :

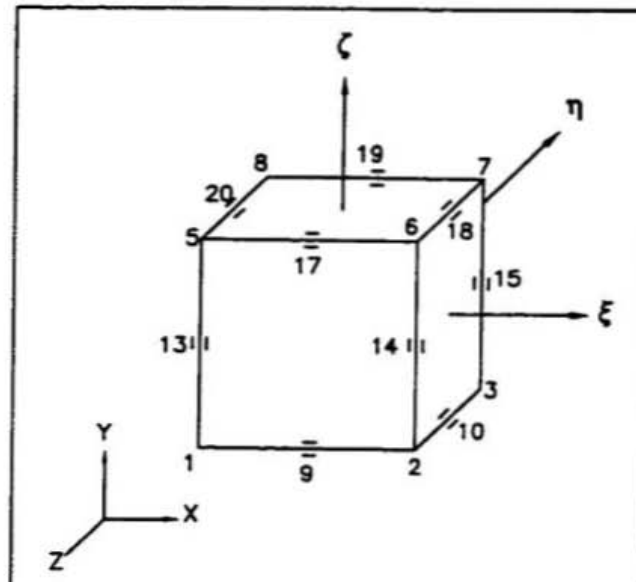

Figure 3.3 3D master element

$$[J] = \begin{bmatrix} \frac{\partial x}{\partial \xi} & \frac{\partial y}{\partial \xi} & \frac{\partial z}{\partial \xi} \\ \frac{\partial x}{\partial \eta} & \frac{\partial y}{\partial \eta} & \frac{\partial z}{\partial \eta} \\ \frac{\partial x}{\partial \zeta} & \frac{\partial y}{\partial \zeta} & \frac{\partial z}{\partial \zeta} \end{bmatrix} \qquad \text{. . (3.39)}$$

The derivatives of shape functions in global coordinates for the evaluation of [B] matrix are given by :

$$\begin{Bmatrix} \frac{\partial N_i}{\partial x} \\ \frac{\partial N_i}{\partial y} \\ \frac{\partial N_i}{\partial z} \end{Bmatrix} = [J]^{-1} \begin{Bmatrix} \frac{\partial N_i}{\partial \xi} \\ \frac{\partial N_i}{\partial \eta} \\ \frac{\partial N_i}{\partial \zeta} \end{Bmatrix} \quad \text{. . (3.40)}$$

The [B] matrix for a second order 3D P-element is partitioned into 20 sub-matrices (corresponding to 8 corner nodes and 12 mid-side hierarchic nodes) and along with a partitioned matrix is given in Eqn.(3.41). Eqn.(3.42) depicts the constitutive relationship which relates the stresses and strains. The steps for formulation and evaluation of the stiffness matrix are the same as for a 2D element.

$$[B] = \langle . \quad . \quad . \quad |B_i| \quad . \quad . \quad . \rangle$$

$$[B_i] = \begin{bmatrix} \frac{\partial N_i}{\partial x} & 0 & 0 \\ 0 & \frac{\partial N_i}{\partial y} & 0 \\ 0 & 0 & \frac{\partial N_i}{\partial z} \\ \frac{\partial N_i}{\partial y} & \frac{\partial N_i}{\partial x} & 0 \\ 0 & \frac{\partial N_i}{\partial z} & \frac{\partial N_i}{\partial y} \\ \frac{\partial N_i}{\partial z} & 0 & \frac{\partial N_i}{\partial x} \end{bmatrix} \quad \text{. . (3.41)}$$

$$\{\sigma^e\} = [D]\{\varepsilon^e\}$$

$$\begin{Bmatrix} \sigma_x \\ \sigma_y \\ \sigma_z \\ \tau_{xy} \\ \tau_{yz} \\ \tau_{zx} \end{Bmatrix} = \frac{E}{(1+\nu)(1-2\nu)} \begin{bmatrix} 1-\nu & \nu & \nu & 0 & 0 & 0 \\ . & 1-\nu & \nu & 0 & 0 & 0 \\ . & . & 1-\nu & 0 & 0 & 0 \\ . & . & . & \frac{1-2\nu}{2} & 0 & 0 \\ . & . & . & . & \frac{1-2\nu}{2} & 0 \\ \text{symm} & . & . & . & . & \frac{1-2\nu}{2} \end{bmatrix} \begin{Bmatrix} \epsilon_x \\ \epsilon_y \\ \epsilon_z \\ \gamma_{xy} \\ \gamma_{yz} \\ \gamma_{zx} \end{Bmatrix} \quad \ldots (3.42)$$

3.4.1 Enriched 3D P-element

As shown by Sih and Liebowitz [27], the displacements u_c', v_c' and w_c' near the edge of the crack in directions x', y' and z' (Fig. 3.4) parallel to the normal, the binormal and the tangent to the crack front are expressed as :

$$\begin{aligned} u_c' &= K_I f_1 + K_{II} g_1 \\ v_c' &= K_I f_2 + K_{II} g_2 \\ w_c' &= K_{III} f_3 \end{aligned} \quad \ldots (3.43)$$

where f_1, etc. are given as :

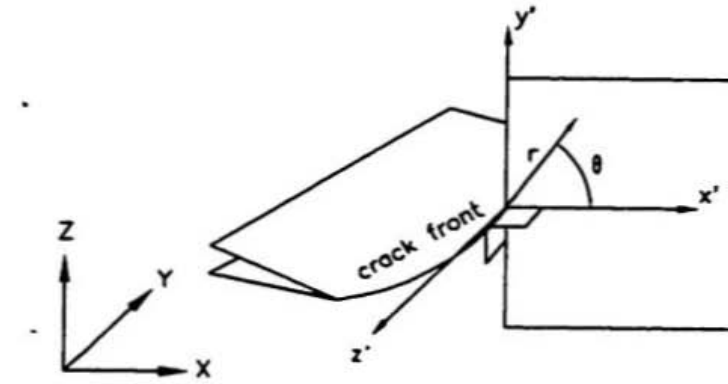

Figure 3.4 Coordinate system at the crack front (3D)

$$f_1 = \frac{1+\nu}{4E}\sqrt{\frac{2r}{\pi}}\left[(5-8\nu)\cos\frac{\theta}{2} - \cos\frac{3\theta}{2}\right]$$

$$g_1 = \frac{1+\nu}{4E}\sqrt{\frac{2r}{\pi}}\left[(9-8\nu)\sin\frac{\theta}{2} + \sin\frac{3\theta}{2}\right]$$

$$f_2 = \frac{1+\nu}{4E}\sqrt{\frac{2r}{\pi}}\left[(7-8\nu)\sin\frac{\theta}{2} - \sin\frac{3\theta}{2}\right] \qquad \text{. . (3.44)}$$

$$g_2 = -\frac{1+\nu}{4E}\sqrt{\frac{2r}{\pi}}\left[(3-8\nu)\cos\frac{\theta}{2} + \cos\frac{3\theta}{2}\right]$$

$$f_3 = \frac{2\,(1+\nu)}{E}\sqrt{\frac{2r}{\pi}}\sin\frac{\theta}{2}$$

The displacements $\mathbf{u}_e'$, etc. are in the local crack coordinate system ($\mathbf{x}'$, $\mathbf{y}'$, $\mathbf{z}'$). For enrichment of the displacement assumption of the P-element, these are transformed into displacements in the global coordinate system, u_e, etc. The transformation matrix, T, is

a 3x3 matrix of direction cosines formed between the local and global coordinate axes.

$$[T] = \begin{bmatrix} T_{x'x} & T_{x'y} & T_{x'z} \\ T_{y'x} & T_{y'y} & T_{y'z} \\ T_{z'x} & T_{z'y} & T_{z'z} \end{bmatrix} \qquad \ldots (3.45)$$

where $T_{11} = T_{x'x}$ = the cosine of the angle between the local x' and global X axes.

The displacements u_c, etc. in the global coordinates are determined from the relationship

$$\begin{Bmatrix} u_c' \\ v_c' \\ w_c' \end{Bmatrix} = [T] \begin{Bmatrix} u_c \\ v_c \\ w_c \end{Bmatrix} \qquad \ldots (3.46)$$

and are given as :

$$\begin{aligned} u_c &= K_I [T_{11} f_1 + T_{21} f_2] + K_{II} [T_{11} g_1 + T_{21} g_2] + K_{III} [T_{31} f_3] \\ &= K_I P_1 + K_{II} Q_1 + K_{III} R_1 \end{aligned} \qquad \ldots (3.47)$$

The displacement interpolation of the enriched 3D P-element is then given by :

$$u^e = [P]\{\alpha\} + K_I P_1 + K_{II} Q_1 + K_{III} R_1 \qquad \ldots (3.48)$$

Using the standard procedure, the second order displacement interpolation in the element in terms of the nodal variables is given by :

$$
\begin{aligned}
u^{e}_{EH} &= \langle N \rangle \{u^{e}\} + K_{I} \left[P_{1} - \sum_{i=1}^{4} N_{i} P_{1i} - \sum_{i=5}^{8} N_{i} P''_{1i}\right] \\
&+ K_{II} \left[Q_{1} - \sum_{i=1}^{4} N_{i} Q_{1i} - \sum_{i=5}^{8} N_{i} Q''_{1i}\right] \\
&+ K_{III} \left[R_{1} - \sum_{i=1}^{4} N_{i} R_{1i} - \sum_{i=5}^{8} N_{i} R''_{1i}\right] \\
&= \langle N \rangle \{u^{e}\} + K_{I} LP_{1} + K_{II} LQ_{1} + K_{III} LR_{1}
\end{aligned}
\qquad \ldots (3.49)
$$

In the 2D enrichment, the additional nodal degrees of freedom are mode I and mode II stress intensity factors. In the 3D case there are three nodes along the crack front, two corner and one mid-side node. Each node is associated with three unknowns, mode I, mode II and mode III stress intensity factors, thus there are 9 additional DOF for a 3D enriched element. The SIF's are assumed to have a quadratic variation along the crack front and this variation is given as :

$$
\begin{aligned}
K_{I} &= M_{1} K_{11} + M_{2} K_{12} + M_{3} K_{13} \\
K_{II} &= M_{1} K_{21} + M_{2} K_{22} + M_{3} K_{23} \\
K_{III} &= M_{1} K_{31} + M_{2} K_{32} + M_{3} K_{33}
\end{aligned}
\qquad \ldots (3.50)
$$

where

$$
\begin{aligned}
M_{1} &= \frac{\beta^{2} - \beta}{2} \\
M_{2} &= 1 - \beta^{2} \\
M_{3} &= \frac{\beta^{2} + \beta}{2}
\end{aligned}
\qquad \ldots (3.51)
$$

K_{ij} in Eqn.(3.50) denotes K_i at node j. The local axes β is equal to the master element axis ζ and lies along the crack front and the z' axis of the crack tip coordinate system. Combining equations (3.49) and (3.50) the displacement interpolation for the enriched element is written as :

$$\begin{aligned} u^e_{EH} = \langle N \rangle \{u^e\} &+ K_{11} A_{11} + K_{21} A_{12} + K_{31} A_{13} \\ &+ K_{12} A_{14} + K_{22} A_{15} + K_{32} A_{16} \\ &+ K_{13} A_{17} + K_{23} A_{18} + K_{33} A_{19} \end{aligned} \quad \ldots (3.52)$$

For the derivation of the [B] matrix let the displacement interpolation for v and w be given by :

$$\begin{aligned} v^e_{EH} = \langle N \rangle \{v^e\} &+ K_{11} A_{21} + K_{21} A_{22} + K_{31} A_{23} \\ &+ K_{12} A_{24} + K_{22} A_{25} + K_{32} A_{26} \\ &+ K_{13} A_{27} + K_{23} A_{28} + K_{33} A_{29} \end{aligned} \quad \ldots (3.53)$$

$$\begin{aligned} w^e_{EH} = \langle N \rangle \{w^e\} &+ K_{11} A_{31} + K_{21} A_{32} + K_{31} A_{33} \\ &+ K_{12} A_{34} + K_{22} A_{35} + K_{32} A_{36} \\ &+ K_{13} A_{37} + K_{23} A_{38} + K_{33} A_{39} \end{aligned} \quad \ldots (3.54)$$

Using equations (3.52) to (3.54), the strains are evaluated as :

$$\{\varepsilon^e\} = [B]\{d^e\} \quad \ldots (3.55)$$

$$\{d^e\}^T = \langle u_1\ v_1\ w_1 \ldots u_{20}\ v_{20}\ w_{20}\ K_{11}\ K_{21}\ K_{31}\ K_{12}\ K_{22}\ K_{32}\ K_{13}\ K_{23}\ K_{33} \rangle$$

and the [B] matrix is given by :

$$[B] = \langle \; . \; . \; . \; |B_i| \; . \; . \; . \; B_{k1} \; B_{k2} \; B_{k3} \rangle$$

$$[B_{ki}] = \begin{bmatrix} \dfrac{\partial A_{11}}{\partial x} & \dfrac{\partial A_{12}}{\partial x} & \dfrac{\partial A_{13}}{\partial A_x} \\ \dfrac{\partial A_{21}}{\partial y} & \dfrac{\partial A_{22}}{\partial y} & \dfrac{\partial A_{23}}{\partial A_y} \\ \dfrac{\partial A_{31}}{\partial z} & \dfrac{\partial A_{32}}{\partial z} & \dfrac{\partial A_{33}}{\partial A_z} \\ \dfrac{\partial A_{21}}{\partial x}+\dfrac{\partial A_{11}}{\partial y} & \dfrac{\partial A_{22}}{\partial x}+\dfrac{\partial A_{12}}{\partial y} & \dfrac{\partial A_{23}}{\partial x}+\dfrac{\partial A_{13}}{\partial y} \\ \dfrac{\partial A_{21}}{\partial z}+\dfrac{\partial A_{31}}{\partial y} & \dfrac{\partial A_{22}}{\partial z}+\dfrac{\partial A_{32}}{\partial y} & \dfrac{\partial A_{23}}{\partial z}+\dfrac{\partial A_{33}}{\partial y} \\ \dfrac{\partial A_{31}}{\partial x}+\dfrac{\partial A_{11}}{\partial z} & \dfrac{\partial A_{32}}{\partial x}+\dfrac{\partial A_{12}}{\partial z} & \dfrac{\partial A_{33}}{\partial x}+\dfrac{\partial A_{13}}{\partial z} \end{bmatrix} \quad . . \textbf{(3.56)}$$

The stiffness matrix for the second order 3D EH-element is then evaluated using the standard procedure described in previous sections.

Chapter IV

COMPUTER IMPLEMENTATION

4.1 Computer Program

A static *p*-version finite element analysis program MUNSID is developed in C language. The capabilities include analysis of plane elasticity and LEFM problems in two and three dimensions. One of the primary aims of this study is to develop and determine the numerical accuracy of the enriched hierarchical elements. The finite elements are quadrilateral shaped so a quadrilateral mesh generator with automatic node numbering and elemental connectivity data generation is also developed for ease of input. The program utilizes *p*-enrichment and the mesh need not be refined for convergence studies. The three main segments of the program are : Elemental stiffness matrix formulation, global assembly of the elemental matrices and the solution routine. Various aspects of MUNSID are discussed in the following sections.

4.1.1 Input

Besides the standard input parameters such as geometrical and physical properties of the problem, the order of the elements, the order of geometric shape functions, plane stress

or plane strain analysis option, the number of iterations and an option for crack tip analysis are also required as input. For 2D crack problems the value of ϕ, orientation of the crack plane w.r.t. the global coordinate axes, and for 3D problems the vector normal to the crack plane are additional input parameters required.

4.1.2 Elemental stiffness matrix evaluation

For most of the analyses the sub-parametric element formulation is utilized. The order of the element is almost always greater than unity as p is successively increased while the element edges are generally straight and therefore the order of the geometric shape functions is one. A maximum geometric order of two is used for problems having curved boundaries. The elements are not defined as iso- or sub-parametric in the strictest sense as the geometric shape functions are not hierarchical but standard serendipity shape functions. Gaussian integration is employed for the evaluation of the stiffness matrices. The (p+1) Gauss integration rule is used to integrate a partitioned sub-matrix K_{ij}, where p is the higher order of the matrix i.e. $p = \max(i,j)$. To avoid zero eigenvalues in the stiffness matrices the reduced integration rule is not used, however, reduced integration for the second order is found valid as long as the element is not enriched further.

4.1.3 Assembly and solution of global stiffness matrix

Since the elements of the global stiffness matrices lie predominantly along the diagonal, to avoid storing a large number of zero elements, each global partitioned matrix is assembled in a skyline format. The Gaussian elimination is used to decompose the diagonal partitioned matrices into the LDL^T form (Bathe[3] Chap. 8), and the off-

diagonal partitioned matrices are utilized for the iterative solution.

4.2 Computational Ease

The use of hierarchical elements results in an improved stiffness matrix that contains lower order stiffness matrix as a sub-matrix. The improved stiffness matrix differs from the previous lower order stiffness matrix in that it contains rows and columns corresponding to the additional nodal variables. Hence the effort spent in triangularizing the previous stiffness matrix is entirely saved and improved solutions are obtained by *ad hoc* iterative procedures. The computational effort required for element matrix generation also depends on the number of integration points and therefore on the degree of the polynomial to be integrated. Usually all shape functions have the same polynomial order and the burden of numerical integration rapidly increases with the order of the polynomial. In the hierarchical approach the number of integration points depends on the order of the (partitioned) stiffness matrix to be computed and in many cases is much lower than that of conventional analysis.

Consider a plane elasticity problem with overall global stiffness matrices K_1, K_2 and K_3 corresponding to first order, second order and third order analysis respectively :

$$[K_1] = [K_{11}] \qquad \ldots(4.1)$$

The stiffness matrix K_{11} is evaluated by the $(p+1=)$ 2 point Gauss quadrature rule. It is then decomposed into the LDL^T form and direct solution is obtained for nodal

$$[K_2] = \begin{bmatrix} K_{11} & K_{12} \\ K_{21} & K_{22} \end{bmatrix} \quad \ldots(4.2)$$

$$[K_3] = \begin{bmatrix} K_{11} & K_{12} & K_{13} \\ K_{21} & K_{22} & K_{23} \\ K_{31} & K_{32} & K_{33} \end{bmatrix} \quad \ldots(4.3)$$

variables corresponding to the first order. K_2 contains K_1 as a sub-matrix and due to the symmetry of the matrix only K_{12} and K_{22} need be evaluated, which is done using 3 point Gauss quadrature rule. Similarly for K_3 only K_{13}, K_{23} and K_{33} need to be evaluated. The system of equations required to be solved for the third order mesh is :

$$\begin{bmatrix} K_{11} & K_{12} & K_{13} \\ K_{21} & K_{22} & K_{23} \\ K_{31} & K_{32} & K_{33} \end{bmatrix} \begin{Bmatrix} U_1 \\ U_2 \\ U_3 \end{Bmatrix} = \begin{Bmatrix} F_1 \\ F_2 \\ F_3 \end{Bmatrix} \quad \ldots(4.4)$$

where U_1 are the (corner) nodal degrees of freedom and U_2, U_3 are the hierarchic nodal degrees of freedom. F_1, F_2 and F_3 are the load vectors corresponding to the degrees of freedom. The iterative solution scheme adopted for higher order matrices is as follows:

Step 1

$$U_1 = [K_{11}^{-1}] \{F_1\}$$

Step 2

$$U_2 = [K_{22}^{-1}] \{F_2 - K_{12}^T U_1\}$$

$$U_1 = [K_{11}^{-1}] \{F_1 - K_{12} U_2\}$$

Iterations are performed until the values of U_1 converge.

Step 3

$$U_3 = [K_{33}^{-1}] \{F_3 - K_{13}^T U_1 - K_{23}^T U_2\}$$

$$U_2 = [K_{22}^{-1}] \{F_2 - K_{12}^T U_1 - K_{23} U_3\}$$

$$U_1 = [K_{11}^{-1}] \{F_1 - K_{12} U_2 - K_{13} U_3\}$$

Sufficient number of iterations are performed for the convergence of solution with the last step being that for U_1.

There are two observations associated with the use of a higher gauss integration rule. Firstly, only the sub-matrix corresponding to the higher order is evaluated at a higher number of gauss points and secondly, the size of the overall matrix is small compared with that of a mesh using standard elements for the same problem due to the use of coarse meshes in *p*-version FEM. In addition, due to faster *p*-convergence rates, high values of *p* are not required reducing the number of degrees of freedom involved.

Chapter V

NUMERICAL STUDIES AND DISCUSSIONS

5.1 Numerical Application

In this chapter the hierarchical and the enriched hierarchical formulations are numerically examined via the program MUNSID. The short cantilever beam problem and Cook's membrane problem having analytical and reference values are analyzed for verification of the 2D P-element. A double edged crack specimen and a slant cracked tensile specimen are used as tests for the 2D EH-element. Different geometries of T-plate welded joints are analyzed for stress concentration factors. Stress intensity factors for different crack depths at the weld toe of a 45° weld profile T-plate joint are obtained and finally the fatigue life of the specimen is estimated. A double edge cracked specimen, a compact tensile specimen and a plate with a semi-circular embedded surface crack are analyzed using 3D EH-elements. The results obtained with very coarse meshes and a small number of degrees of freedom are in remarkable agreement with the reference values for all cases.

5.2 Tests for 2D P-Element

The cantilever beam and Cook's membrane problems are analyzed and the results obtained validate the formulation of the P-elements and the program MUNSID.

5.2.1 Short cantilever beam problem

A shear loaded cantilever beam is selected as a test problem by many authors [28,29,30,31]. The elasticity solution (Tomishenko and Goodier [32]) for the tip displacement of the problem shown in Fig. 5.1 is :

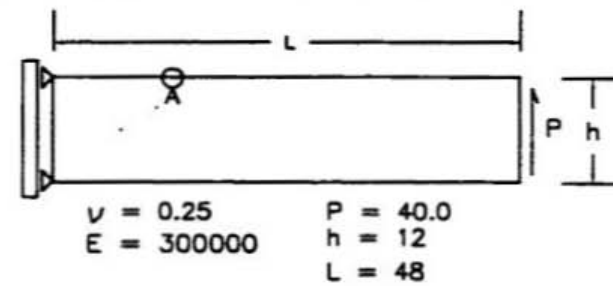

Figure 5.1 Cantilever beam problem

$$v_{tip} = \frac{PL^3}{3EI} + \frac{(4+5\nu)\ PL}{2Eh} = 0.3558 \qquad ..(5.1)$$

The finite element solution is obtained for a mesh of one element, a coarse mesh of four square elements and successively finer meshes constructed by bisection. A distorted four element mesh after MacNeal and Harder [30] is also studied. The results are presented for the tip displacement as well as for bending stress at A (x=12, y=6) for increasing order p till convergence is achieved, where p is the order of the entire mesh. In addition the reduced integration (RI) results for $p=2$ using 2x2 gauss points are also presented. The meshes are shown in Fig. 5.2 and results in Table 5.1 and Table 5.2.

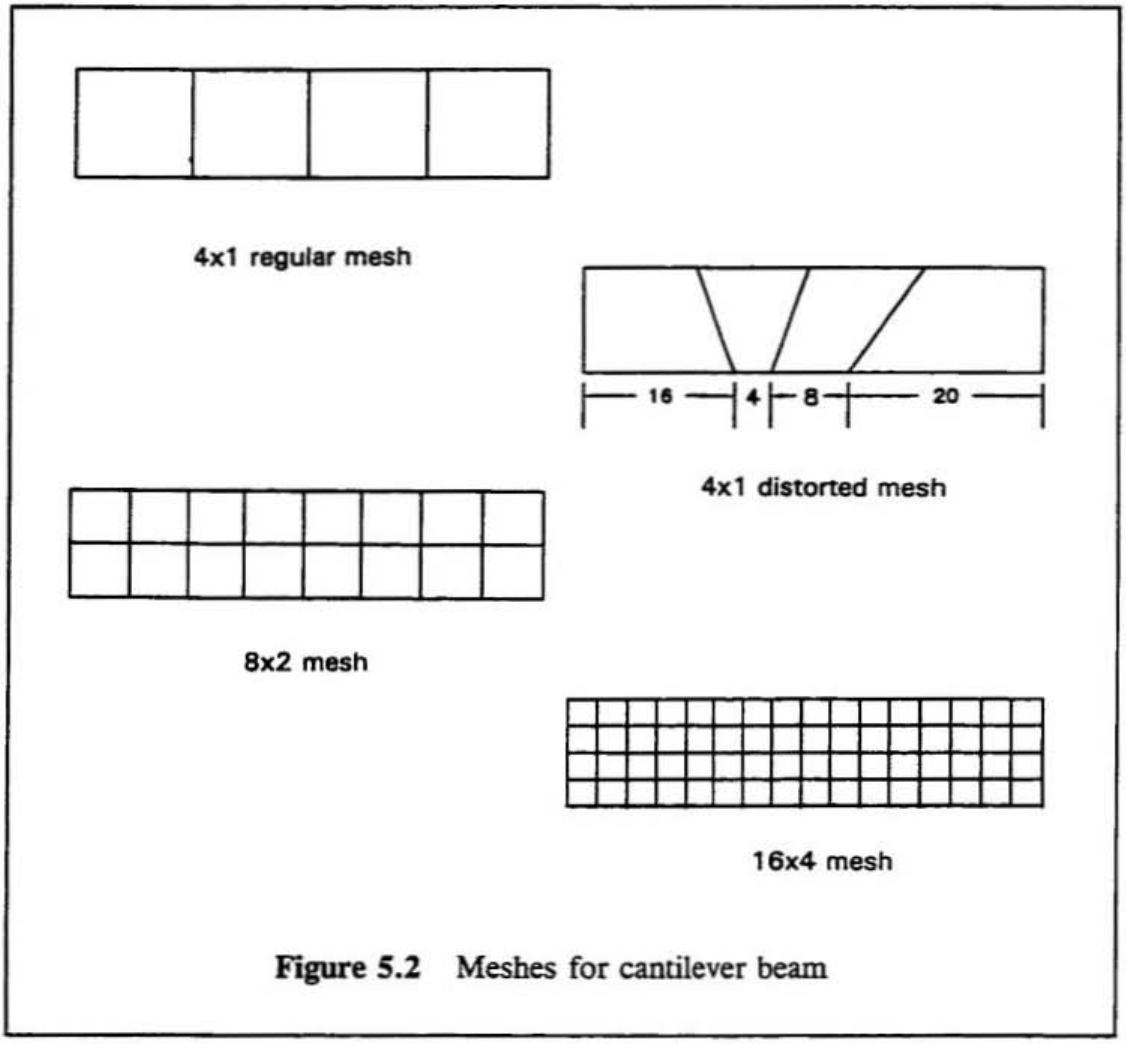

Figure 5.2 Meshes for cantilever beam

Table 5.1 Cantilever Beam Problem (reference and comparison values)

Mesh size	Allman	Ibrahimbegovic	Allman
		v_{tip}	σ_x (x=12,y=6)
4x1	0.3026	0.3445	52.7
8x2	0.3394	0.3504	58.4
16x4	0.3512	0.3543	59.7
4x1-d	-	0.3066	-
Reference		0.3558	60.0

Table 5.2 Cantilever beam problem (results)

Mesh Size	v_{tip}				σ_x (x=12,y=6)			
	RI	$p=2$	$p=3$	$p=4$	RI	$p=2$	$p=3$	$p=4$
1x1	0.3393	0.2989	0.3414	0.3415	59.99	49.53	60.35	60.35
4x1	0.3500	0.3495	0.3522	0.3522	60.0	59.85	60.32	60.13
8x2	0.3558	0.3554	0.3559	0.3559	60.0	59.96	58.66	58.94
16x4	0.3556	0.3557	0.3557	0.3557	59.98	60.0	60.00	60.00
4x1-d	0.3520	0.3534	0.3562	0.3562	57.99	59.0	58.91	58.46

Discussions

1. For any given mesh, the NDOF involved in the analysis by Allman [28] and Ibrahimbegovic [31] is nearly the same as that in MUNSID for $p=2$ and $p=3$ respectively. In comparison, considerably improved results are obtained with MUNSID.

2. For P-elements (Table 5.2), reduced integration results are better than full integration, except for the 16x4 and the distorted 4x1 mesh (4x1-d). Therefore for real life situations involving irregular shaped elements, full integration is preferable.

3. Convergence of results is observed at higher orders for coarse meshes and vice-versa.

4. Even the single element mesh performs quite accurately with a final error of only 4% in displacement and 0.6% in stress. For the 4x1 and 8x2 meshes, the error in tip displacement for both the meshes is 1% and the error in stress is 0.2% and 1% respectively. "Exact" value of stress and a high accuracy of 99.97% in displacement is obtained with the 16x4 mesh for all orders. For a reasonable accuracy, the 4x1 mesh with $p=3$ is sufficient for the analysis.

5.2.2 Cook's membrane problem

A trapezoidal membrane with a shear dominated behaviour proposed by Cook [33] shown in Fig. 5.3 is a test problem for the accuracy of quadrilateral elements. The results for the tip displacement at point C are compared with a reference value of 23.91, obtained by Bergan and Fellipa [29] using a 32 x 32 mesh. The various meshes considered are given in Fig. 5.4 and the results for the tip displacement and the values of stress at the lower (A) and upper (B) mid-sections of the membrane are presented in Table 5.3 and Table 5.4.

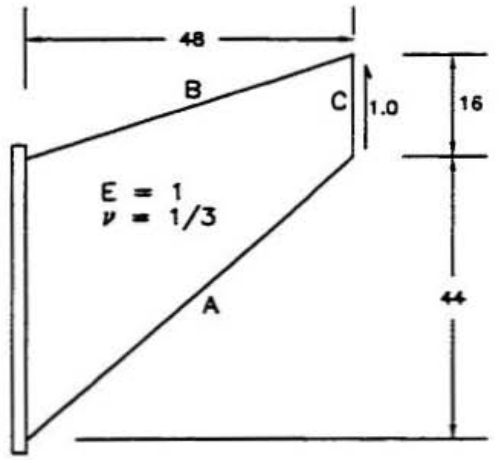

Figure 5.3 Cook's membrane problem

Table 5.3 Cook's membrane problem (reference and comparison values)

Mesh size	Allman	Ibrahimbegovic	Allman	
	v_{tip}		σ_{maxA}	σ_{maxB}
2x2	20.27	20.68	0.1825	-0.1716
4x4	22.78	22.99	0.2261	-0.1921
8x8	23.56	23.66	0.2340	-0.2004
Reference	23.91		0.2359	-0.2012

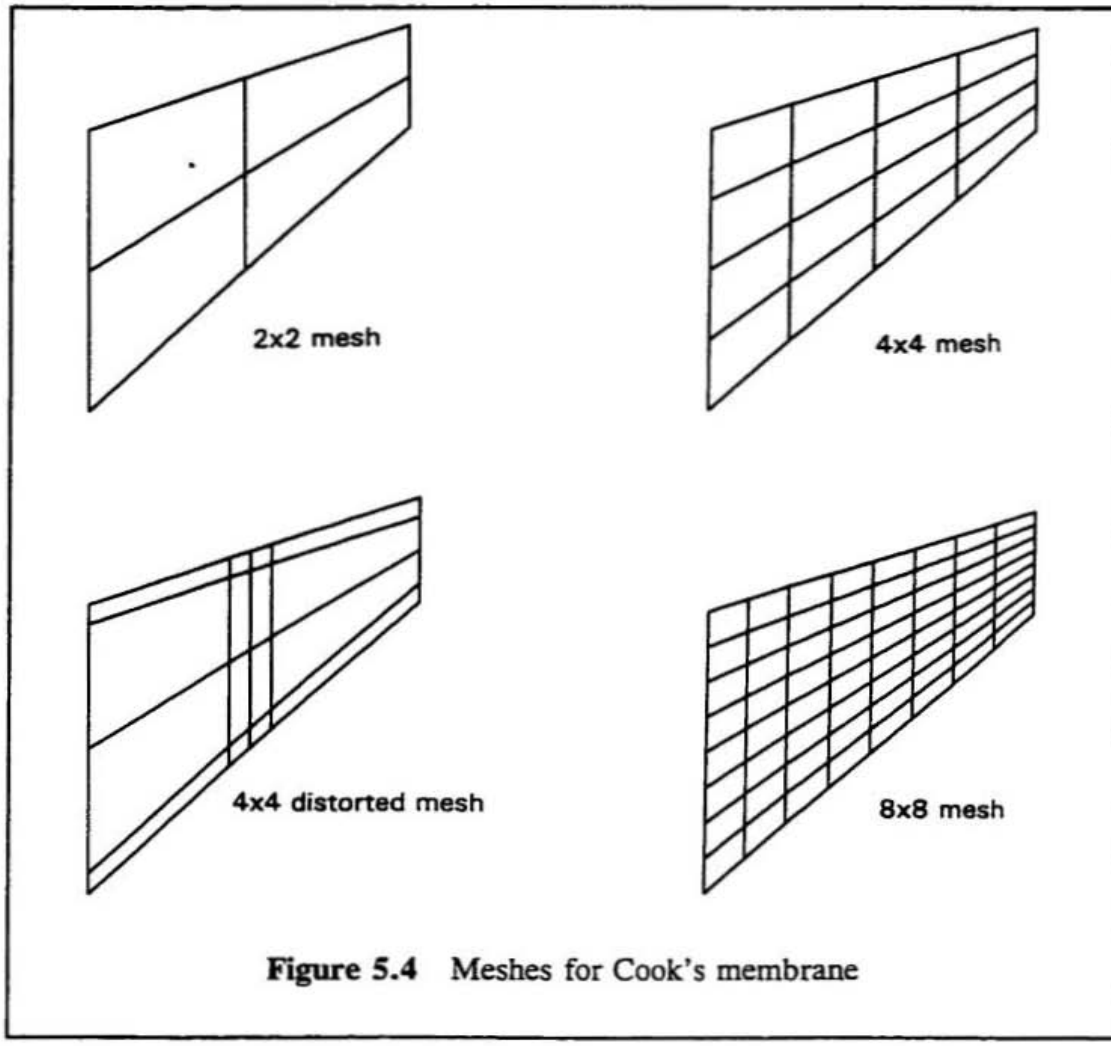

Figure 5.4 Meshes for Cook's membrane

Table 5.4 Cook's membrane problem (results)

Mesh Size	v_{tip}				σ_{maxA} : σ_{maxB}			
	RI	$p=2$	$p=3$	$p=4$	RI	$p=2$	$p=3$	$p=4$
2x2	23.17	23.06	23.47	23.47	0.262 -0.234	0.250 -0.234	0.224 -0.217	0.228 -0.221
4x4	23.73	23.73	23.75	23.75	0.244 -0.202	0.242 -0.201	0.235 -0.201	0.235 -0.201
8x8	23.88	23.88	23.88	23.88	0.239 -0.204	0.239 -0.204	0.236 -0.204	0.236 -0.204
4x4-d	-	23.57	23.82	23.83	- -	0.232 -0.203	0.232 -0.202	0.232 -0.202

Discussions

1. Improved displacements results are obtained for all meshes compared with those by Allman and Ibrahimbegovic. The accuracy of the 2x2 mesh with $p=3$ is nearly equal to, and that of the 4x4 mesh with $p=2$ is greater than, the displacement results by [28] and [31] for an 8x8 mesh. This results in a major decrease in the NDOF involved.

2. The error in the tip displacement is less than 2% for a coarse 2x2 mesh. A high accuracy of 99.87% in displacement results is achieved with an 8x8 mesh. It is also observed for the refined (8x8) mesh that the values of displacement do not vary with increasing order, suggesting convergence of the results.

3. Improved results are also obtained for the maximum principal stress at locations A and B. The 2x2 mesh with $p=2$ performs slightly better than the same mesh by Allman and the accuracy increases considerably as p is increased to 4. The errors for σ_{maxA} are only 0.60% and 0.25%, and for σ_{maxB} are only 0.10% and 1.30%, for the 4x4 and 8x8 meshes respectively. It is noted however that the reference values are also numerically computed and that Ibrahimbegovic did not provide results for stresses which are quite critical for this shear dominated test.

4. The 4x4-d distorted mesh is graded, to improve results, towards points A and B in a geometric progression with a ratio of 0.15 and it includes large aspect ratio elements. Improved displacement results and similar stress results are obtained compared with the 4x4 mesh. It is also analyzed to show the relative flexibility of mesh design in p-version FE analysis.

5.3 Tests for 2D EH-Element

5.3.1 Double edge cracked tensile specimen

The test problem is shown in Fig. 5.5 along with the physical and geometrical properties and the loading conditions. In the construction of meshes, the crack tip is surrounded by EH-elements and the rest of the geometry is modelled by P-elements. The symmetry of the problem is considered and only the upper two quadrants are modelled. Utilizing the symmetry about the crack tip gives slightly erroneous results hence is not considered. The meshes consisting of 4, 8, 12 and 18 elements are shown in Fig. 5.6 along with the results obtained. This problem is also solved by Gifford and Hilton [23] and the plane strain reference value for K_I equal to 2.00 is taken from Brown and Strawley [34].

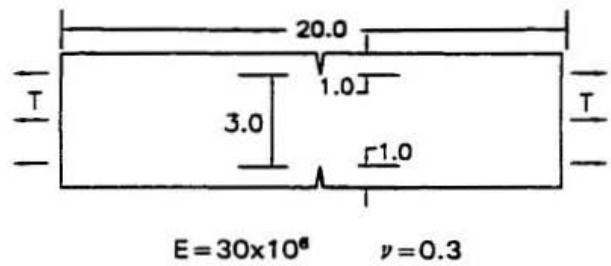

Figure 5.5 Double edge cracked tensile specimen

A mesh for the same problem by Barsoum [19] using 115 elements and employing distorted triangular serendipity isoparametric finite elements to represent the crack tip region is shown in Fig. 5.7 for comparison.

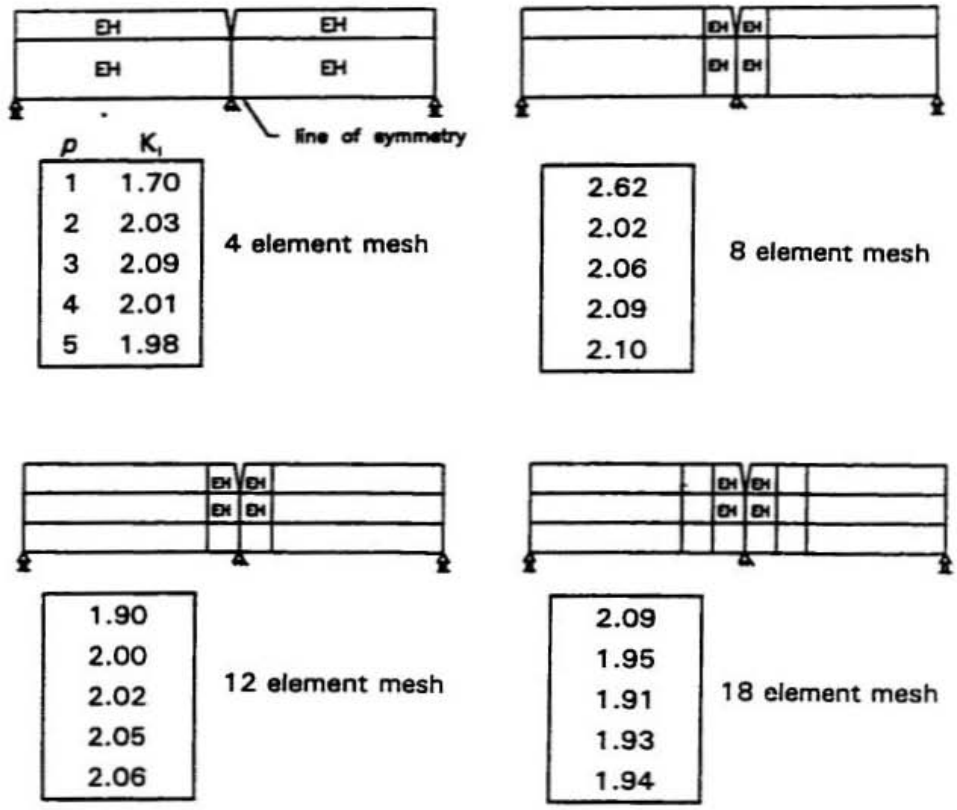

Figure 5.6 Meshes and results for double edge cracked specimen

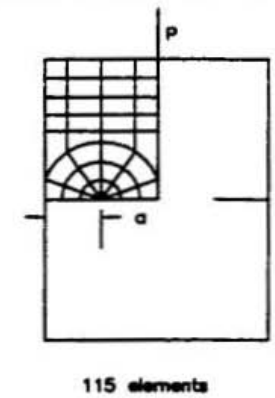

Figure 5.7 Mesh of distorted serendipity elements (Barsoum)

Discussions

1. The maximum order required for convergence for all meshes is 4.

2. The error in the value of stress intensity factor obtained from the four different meshes is less than ±5% which is reasonably accurate

considering the number of degrees of freedom involved, 220, compared to a 700 degree of freedom model by Barsoum (Fig. 5.7).

5.3.2 Slant cracked tensile specimen

The test problem is given in Fig. 5.8. Four different finite element idealizations also considered by Gifford & Hilton [23] are shown in Fig. 5.9 and the plane strain reference values for K_I and K_{II} taken from graphs provided by Bowie [35] are 1.86 and 0.88 respectively. The results are presented along with the meshes in Fig. 5.9.

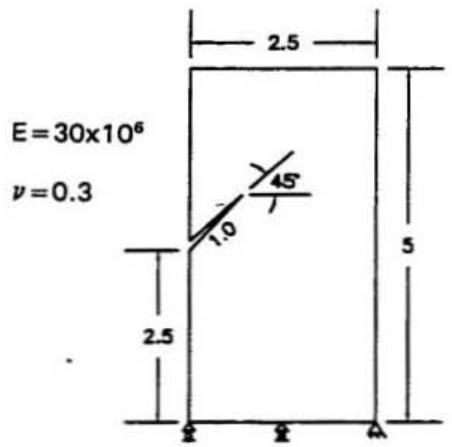

Figure 5.8 Slant cracked tensile specimen

Discussions

1. The values of K_I and K_{II} for each mesh converge at $p=4$. A note for all mesh enrichments is that the order of the elements is not increased selectively rather over the entire domain.

2. For the 4, 7 and 10 element meshes the error is less than 5% in K_I and less than 11% in K_{II}. The 18 element mesh gives quite accurate results with errors of only 2.2% and 1.13% in K_I and K_{II} respectively.

3. The apparent reason for the better performance of the 18 element mesh is the use

of small and regular sized EH-elements at the crack tip.

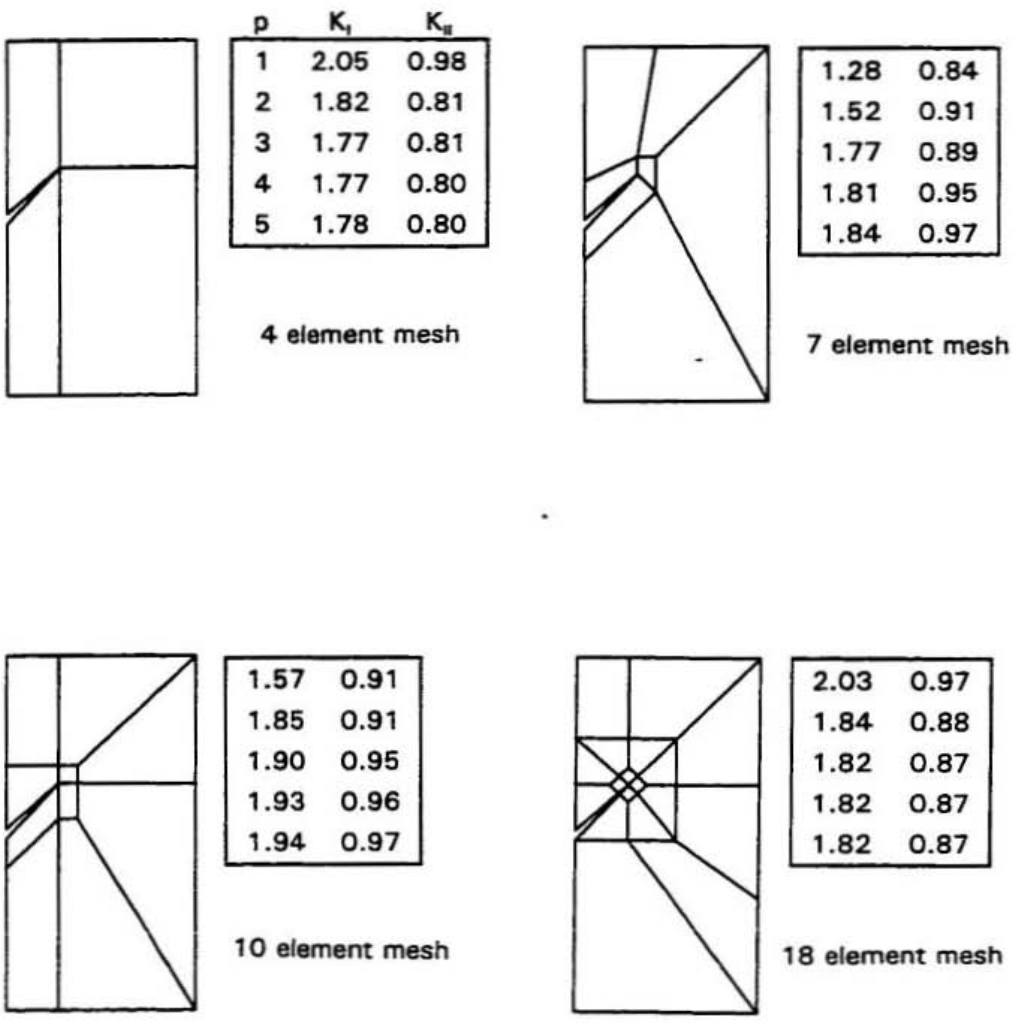

Figure 5.9 Meshes and results for slant cracked tensile specimen

5.4 Analysis of T-Plate Weld Joint

The T-plate joint having base plate thickness, T, and attachment plate thickness, t, with 45° and AWS weld profiles is shown in Fig 5.11. The finite element idealization is done utilizing the symmetry of the problem and the weld joint is tested for stress concentration factors at the weld toe and stress intensity factors for a cracked weld toe. The results are compared with those obtained by Bell [26] using 8-noded isoparametric elements. Various meshes were considered but results presented are for meshes that are the coarsest possible for a reasonable accuracy.

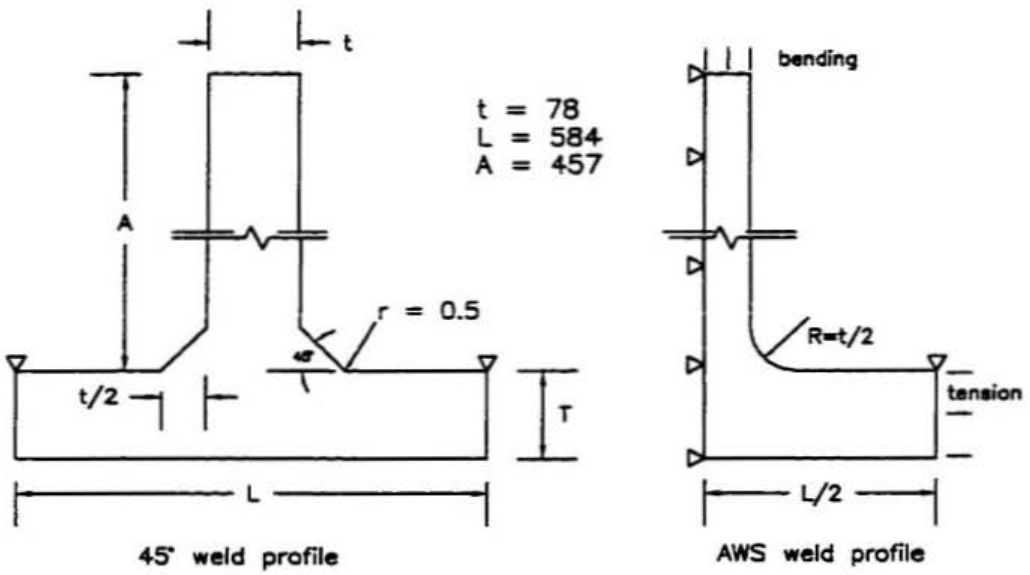

Figure 5.10 Geometry of T-plate weld joint

5.4.1 Stress concentration factors

Stress concentration factors are evaluated for the 45° and AWS weld profiles for two different base-plate to attachment-plate thickness ratios, t/T, of 1.0 and 0.75 with the attachment plate thickness of 78 mm. Tests are done for both three point bending and tensile loadings. The topology is discretized by coarse meshes with three layers of elements graded in geometric progression towards the stress concentration region (the weld toe). The meshes considered for 45° and AWS weld profile with t/T ratio of 1.0 are shown in Fig. 5.12. The value of the weld toe radius, r, is kept equal to 0.5 mm, the same as that selected by Bell. The stress profiles along the base plate thickness direction at the weld toe are also compared with those obtained by Bell. The stress profiles are obtained for loads applied such that the maximum nominal stress has a value of 1.0 at the weld toe. The SCF results are given in Table 5.5*a* & *b* and Table 5.6*a* & *b* and the stress profiles are plotted in Fig. 5.12 to Fig. 5.19.

Table 5.5*a* Stress concentration factor, 45° weld profile, bending load

t/T	Bell	MUNSID					
		$p=1$	$p=2$	$p=3$	$p=4$	$p=5$	$p=6$
1.0	*4.66*	6.205	4.99	4.69	4.52	4.56	4.61
0.75	*5.08*	6.64	5.42	5.10	4.94	4.98	5.05

Table 5.5*b* Stress concentration factor, AWS weld profile, bending load

t/T	Bell	MUNSID					
		$p=1$	$p=2$	$p=3$	$p=4$	$p=5$	$p=6$
1.0	*1.475*	2.25	1.802	1.675	1.62	1.605	1.605
0.75	*1.561*	2.38	1.93	1.79	1.74	1.73	1.73

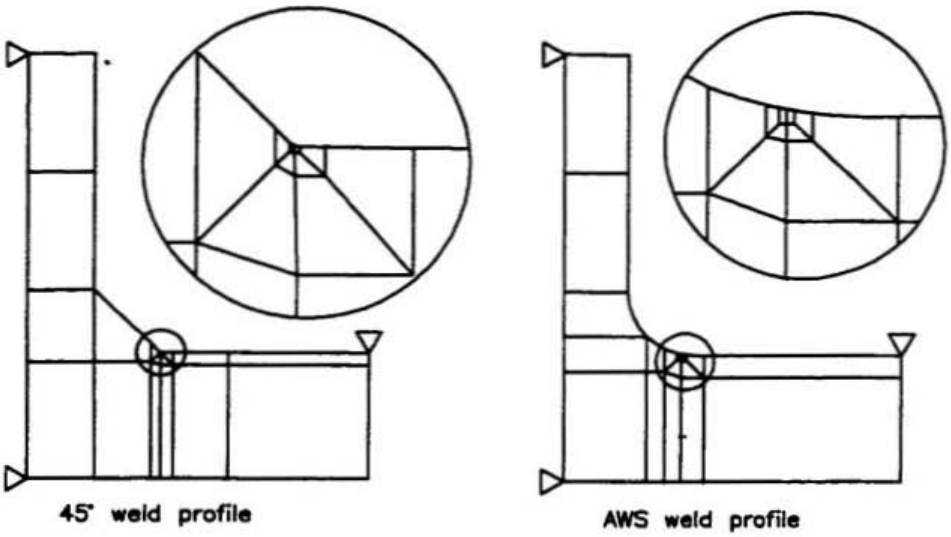

Figure 5.11 Meshes for stress concentration factor evaluation

Table 5.6*a* Stress concentration factor, 45° weld profile, tensile load

t/T	Bell	MUNSID					
		$p=1$	$p=2$	$p=3$	$p=4$	$p=5$	$p=6$
1.0	*3.588*	5.07	4.12	3.94	3.78	3.81	3.87
0.75	*3.912*	5.63	4.47	4.27	4.11	4.145	4.22

Table 5.6*b* Stress concentration factor, AWS weld profile, tensile load

t/T	Bell	MUNSID					
		$p=1$	$p=2$	$p=3$	$p=4$	$p=5$	$p=6$
1.0	*1.341*	1.75	1.52	1.49	1.44	1.43	1.43
0.75	*1.394*	1.91	1.63	1.58	1.54	1.53	1.53

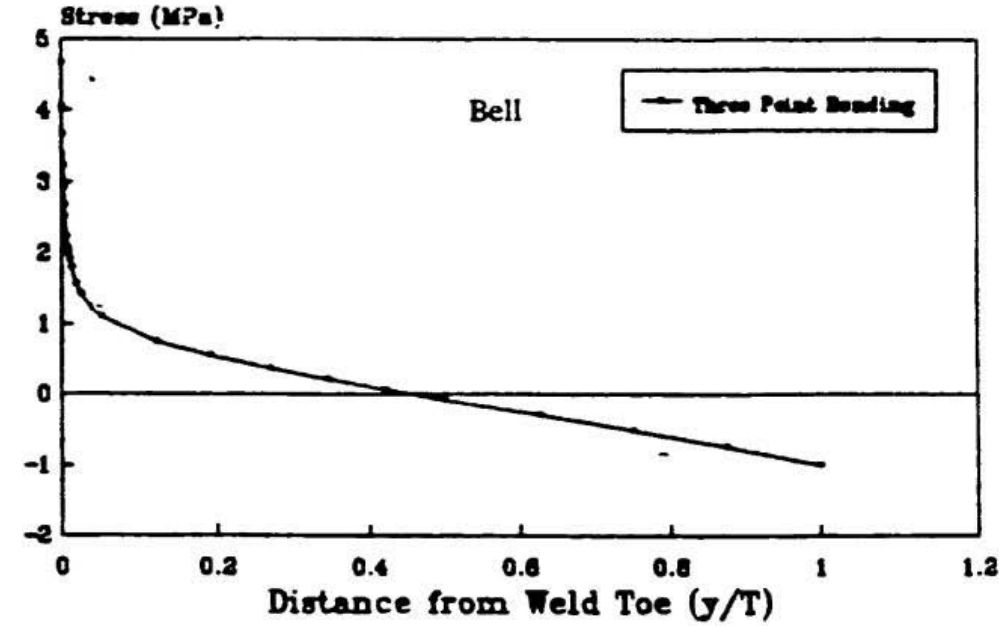

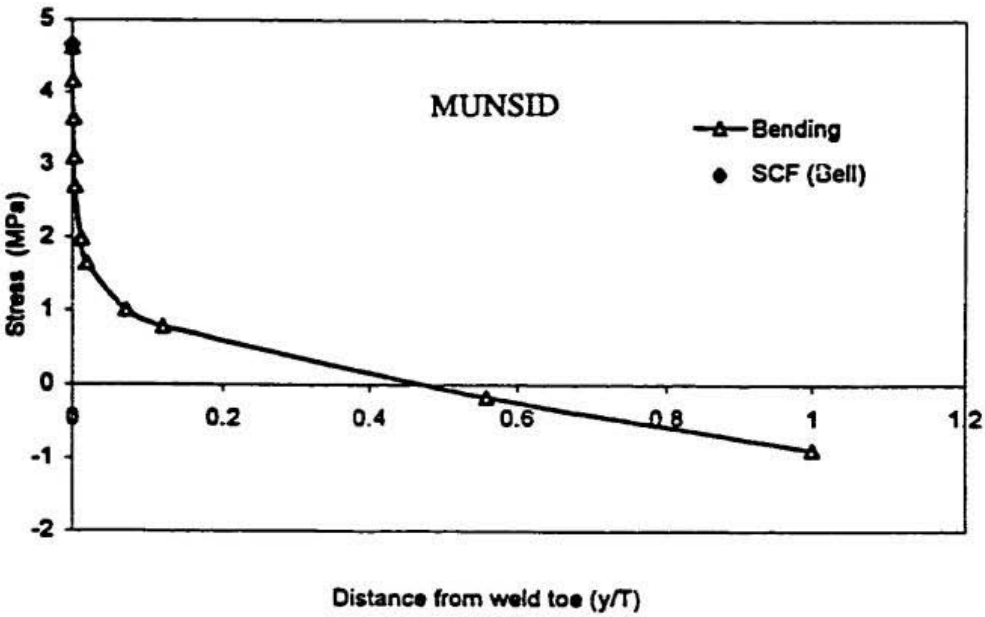

Figure 5.12 Stre distribution through thickness
t=78mm t/T=1.0 45° weld profile

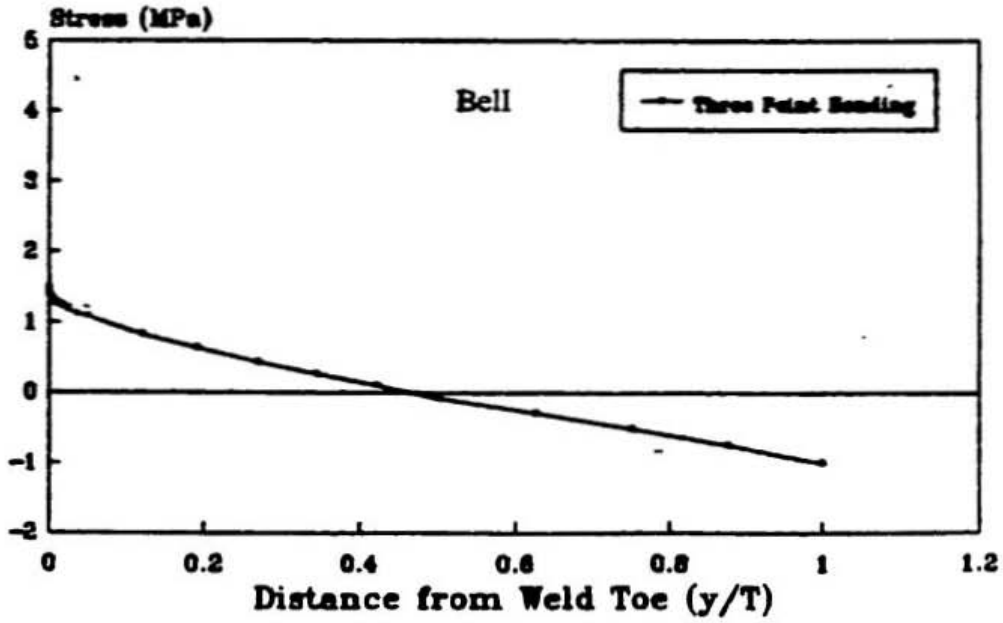

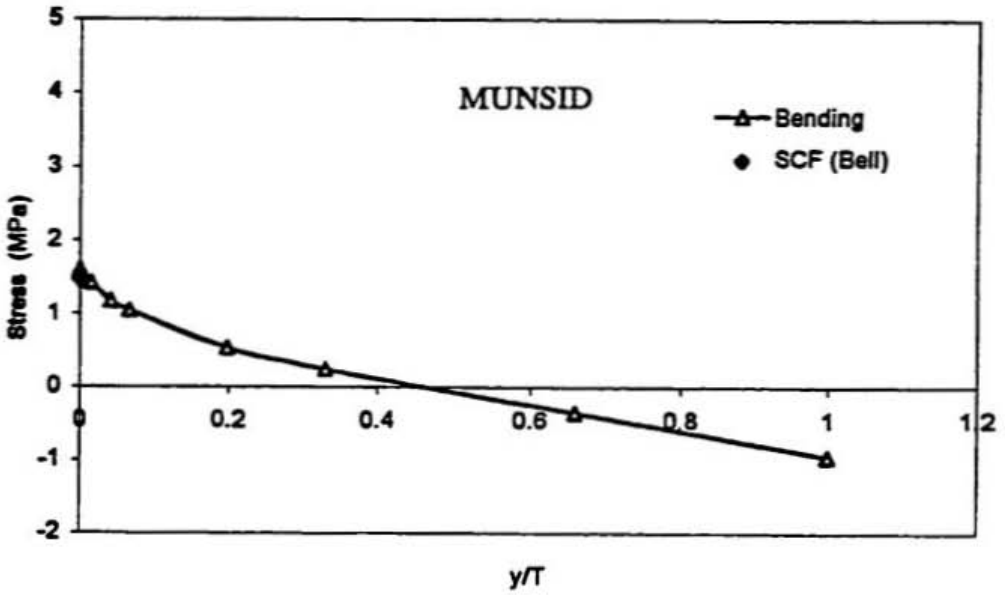

Figure 5.13 Stress distribution through thickness
t=78mm t/T=1.0 AWS weld profile

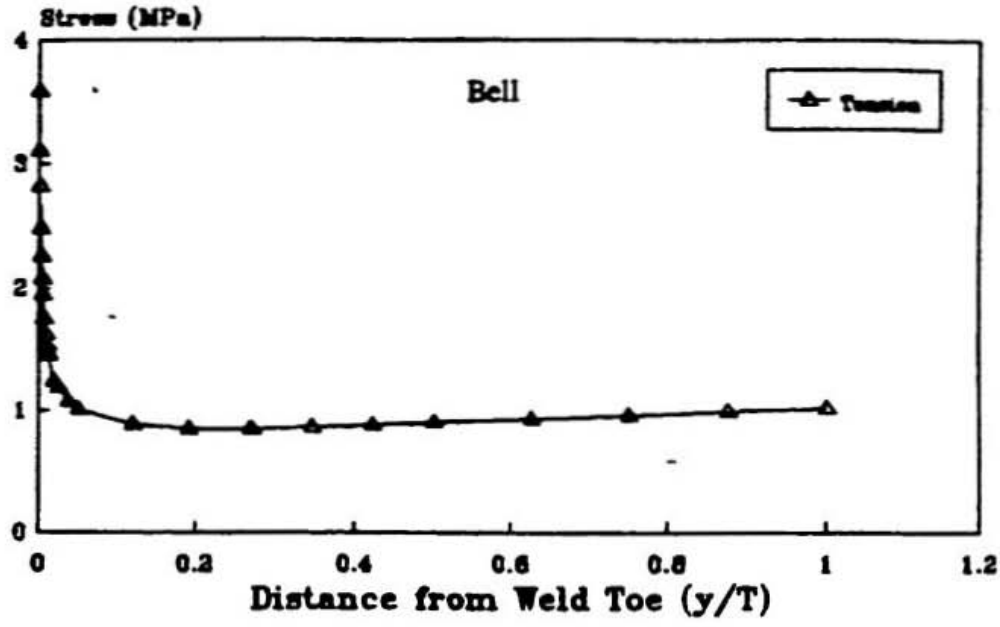

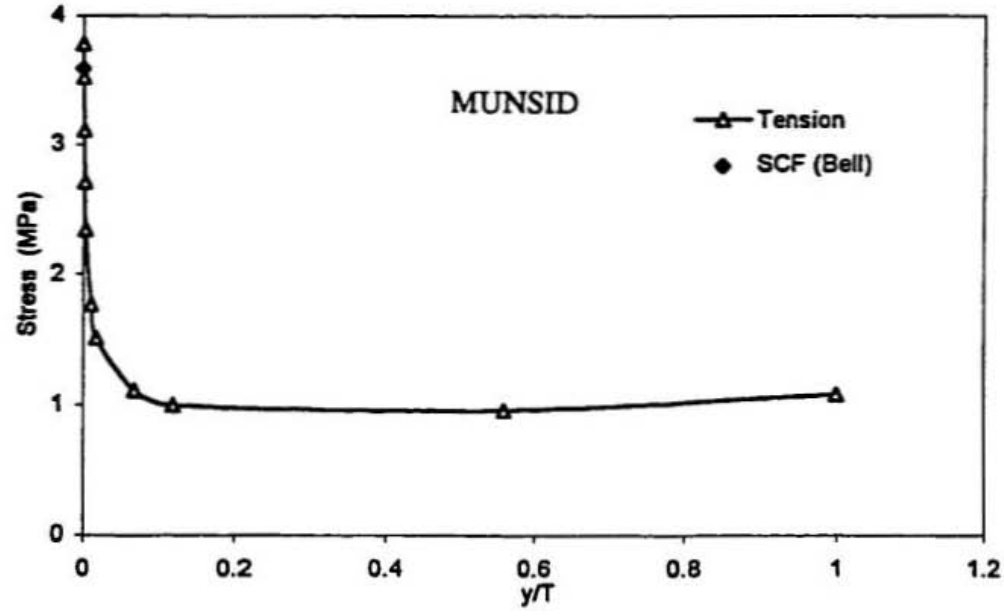

Figure 5.14 Stress distribution through thickness
t=78mm t/T=1.0 45° weld profile

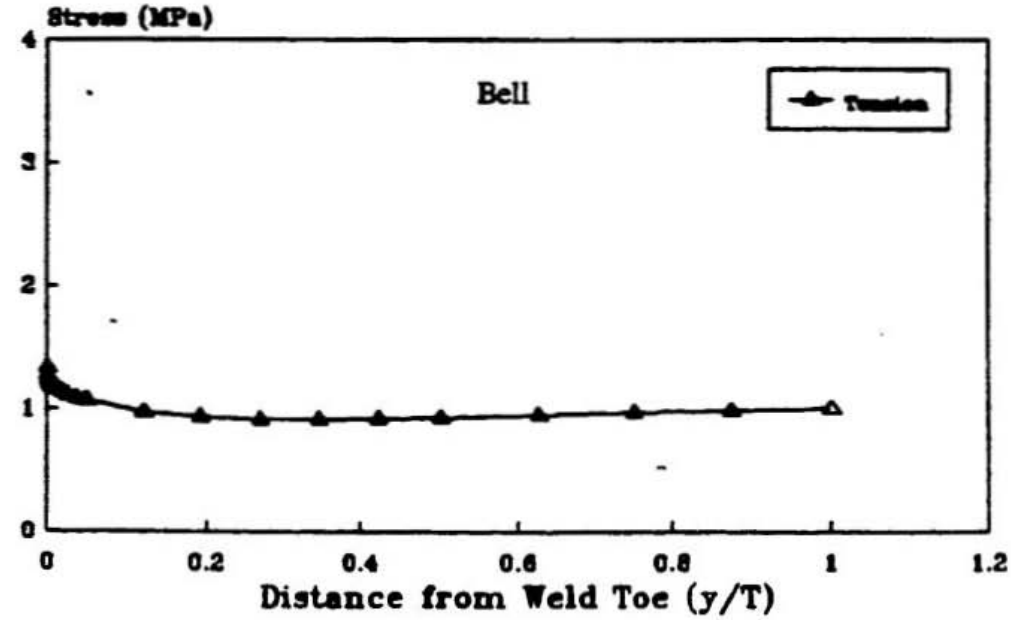

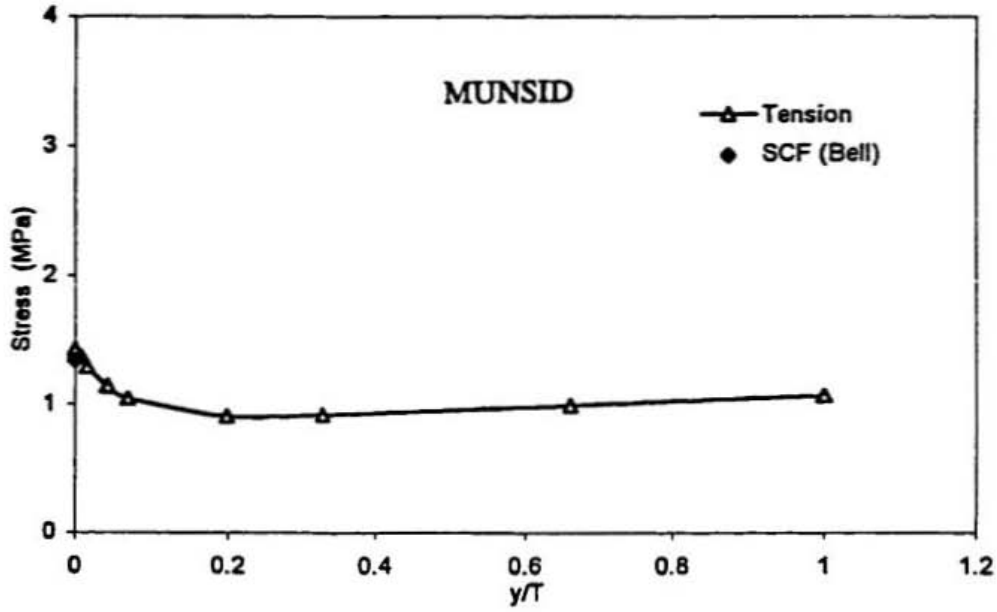

Figure 5.15 Stress distribution through thickness
t=78mm t/T=1.0 AWS weld profile

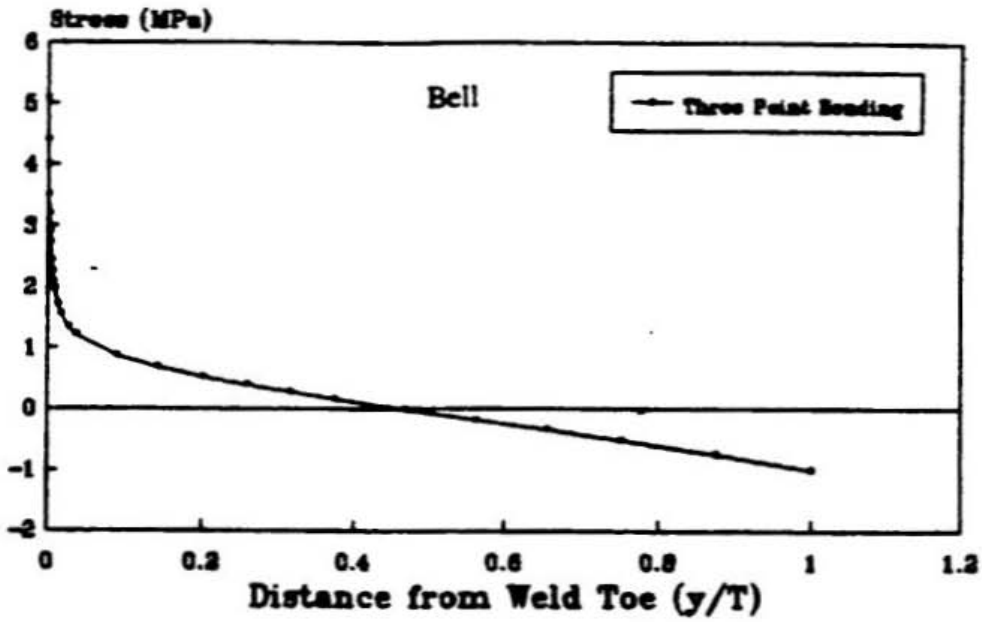

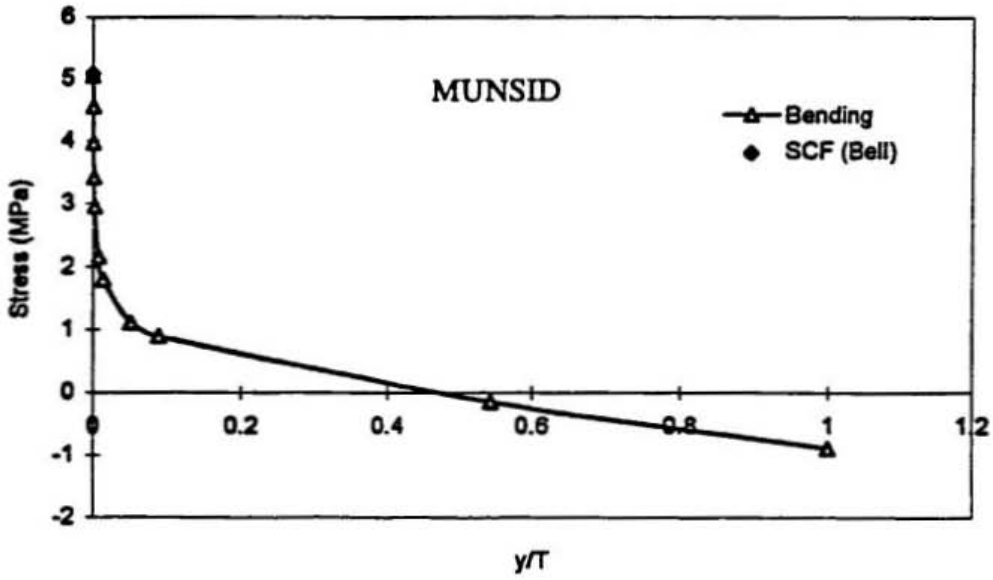

Figure 5.16 Stress distribution through thickness
t=78mm t/T=0.75 45° weld profile

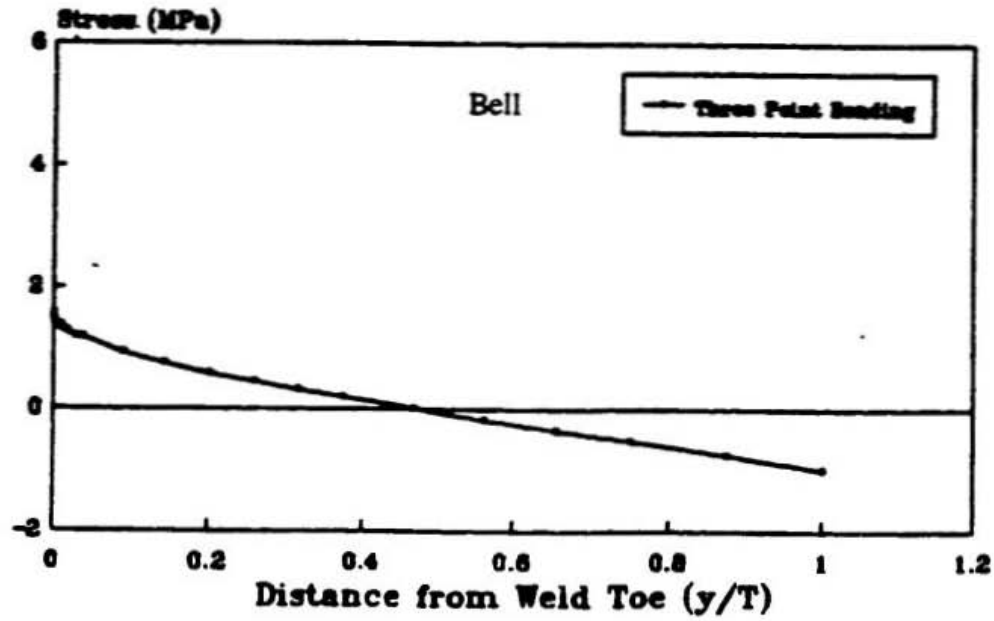

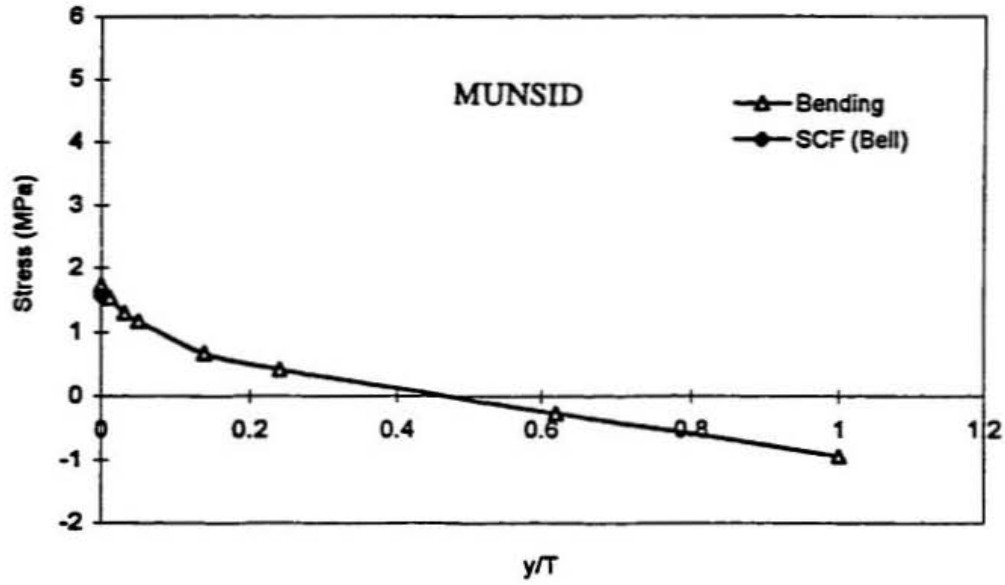

Figure 5.17 Stress distribution through thickness
t=78mm t/T=0.75 AWS weld profile

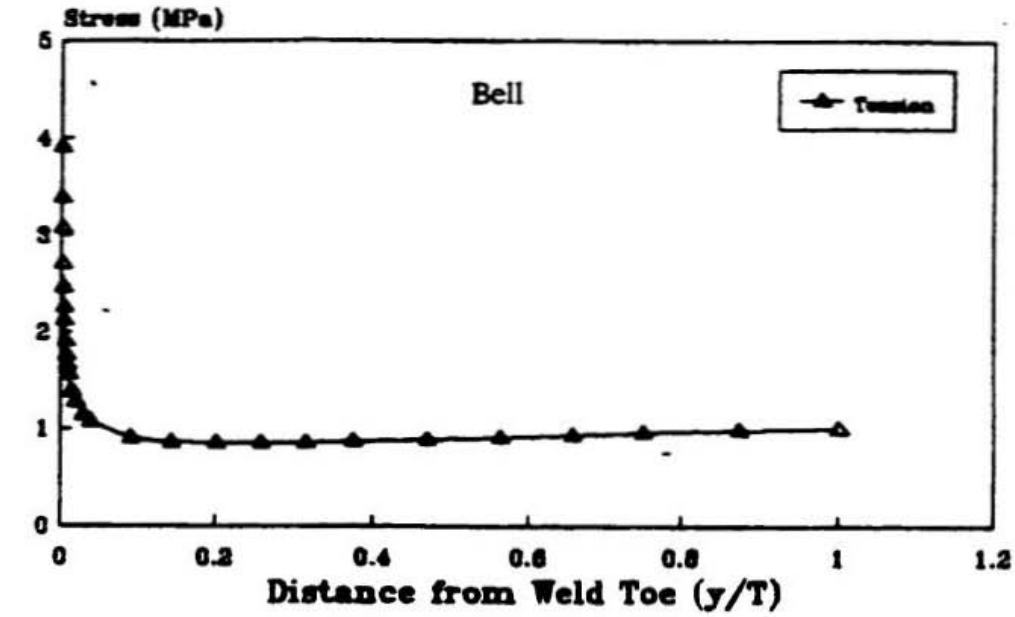

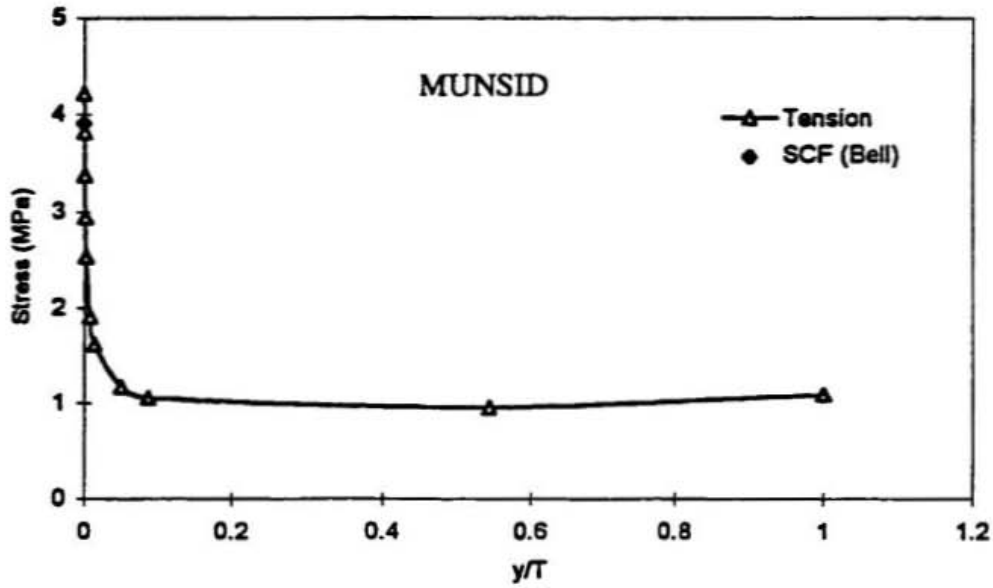

Figure 5.18 Stress distribution through thickness
t=78mm t/T=0.75 45° weld profile

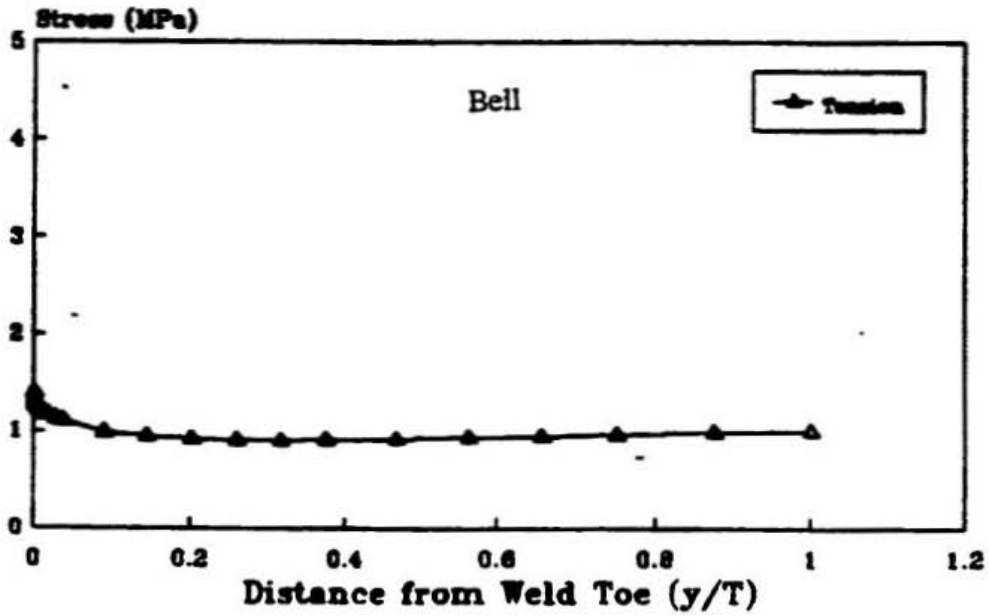

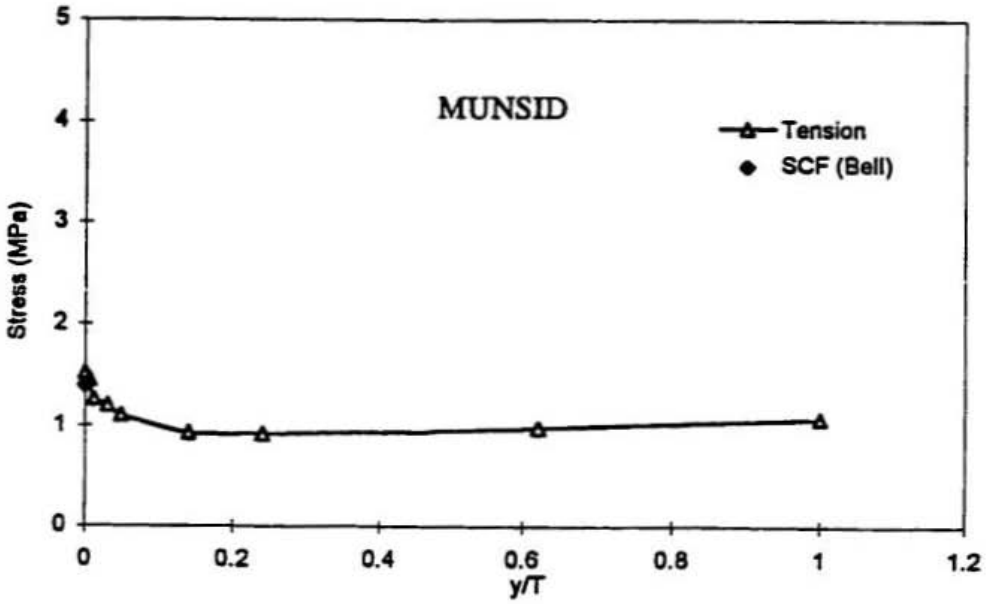

Figure 5.19 Stress distribution through thickness
t=78mm t/T=0.75 AWS weld profile

Discussions

1. The meshes used for the 45° and AWS weld profiles (for both t/T ratios) contain 22 and 21 elements respectively. The meshes are very coarse in the overall domain and graded in a geometric progression at and towards the stress concentration region with a ratio of about 0.15. Reasonably accurate results are obtained with a few degrees of freedom, typically about 600, for a 20-22 element mesh with $p=6$. Bell states in his report "*the joints were modelled using quadratic isoparametric elements and the mesh was highly refined at the weld toe region to insure a smooth radius at the root of the notch and to obtain an accurate value of stress in this region*". In the present study, two P-elements are used to model the root notch radius with geometric shape functions of order two. Reference [36] used a refined mesh for stress concentration factors of a welded joint with about a 100 elements ($\sim$680 degrees of freedom) in a 1 mm^2 area at just the weld toe region.

2. The SCF's obtained in this study (Tables 5.5 and 5.6) are comparable to those obtained by Bell.

3. The stress profiles (Fig. 5.12 to Fig 5.19) are remarkably similar to those given by Bell, and are obtained using only five P-elements along the thickness direction of the base plate at the weld toe. The stresses are obtained by nodal averaging.

5.4.2 Stress intensity factors

The crack growth curve for a T-plate joint with 45° weld profile and t/T ratio of 1.0 with t=78 mm has a 2D reference solution in [26]. Hence this geometry is analyzed for SIF's for different crack depths at the weld toe under three point bending load. The

initial crack depth is taken as 0.5 mm and the final crack depth is taken as T/2 (39 mm). The meshes used for the analysis are given in Fig. 5.20.

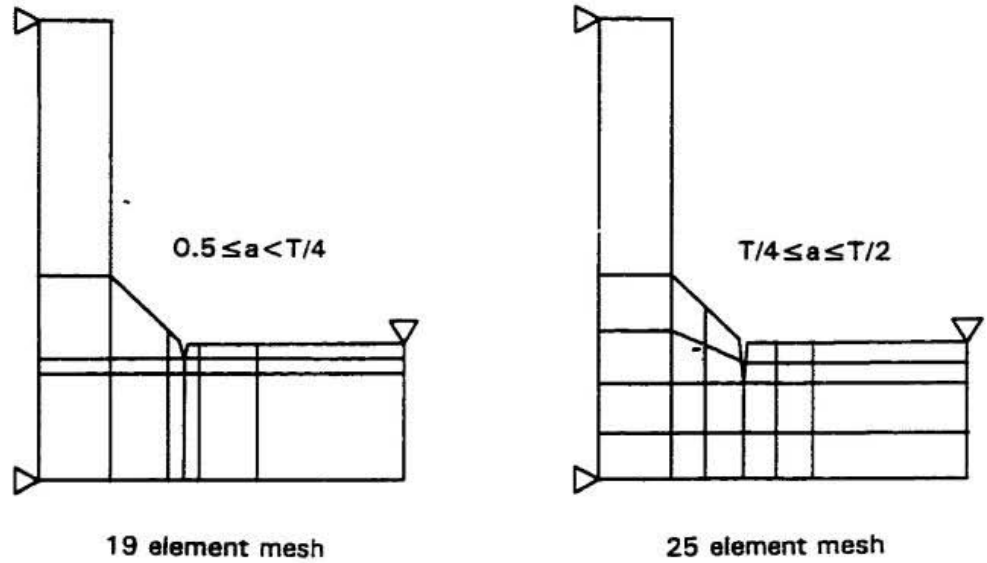

Figure 5.20 Meshes for SIF for 45° weld profile, t/T=1.0

Table 5.7 SIF (MPa√mm) vs crack depth

Crack Depth (mm)	$p=1$	$p=3$	$p=5$
0.5	3.11	3.81	4.01
1.0	3.80	4.59	4.64
5.0	5.22	6.34	6.34
10.0	6.90	7.56	7.62
20.0	11.62	9.61	9.63
30.0	13.62	12.92	12.95
39.0	16.57	17.95	18.02

An empirical relationship is established for the SIF versus crack depth and are plotted

in Fig. 5.21. This empirical value of K (in MPa$\sqrt{m}$) as a function of crack depth a (in metres) is determined by polynomial curve fitting as :

$$K(a) = 12409.65\ a^3 - 618.903\ a^2 + 16.729\ a + 0.1243 \qquad ..(5.2)$$

Eqn.(5.2) is used to evaluate the crack propagation curve (Fig. 5.23) and the fatigue life of the specimen. The constants C and m used in the Paris' equation are those used by Bell. The crack growth rate (Paris equation) and fatigue life (N cycles) are given by:

$$\frac{da}{dN} = C\ (\Delta K)^m = C\ (\Delta \sigma)^m\ K^m$$

$$N = \frac{1}{C\ (\Delta \sigma)^m} \int_{a_i}^{a_f} \frac{da}{K^m} \qquad ..(5.3)$$

$$= \frac{1}{(5.36\ .\ 10^{-12})\ (100)^3} \int_{0.0005}^{0.039} \frac{da}{K(a)^3}$$

The fatigue life is evaluated and compared with that obtained by Bell for a straight fronted crack (SFC) analysis (Fig. 5.22).

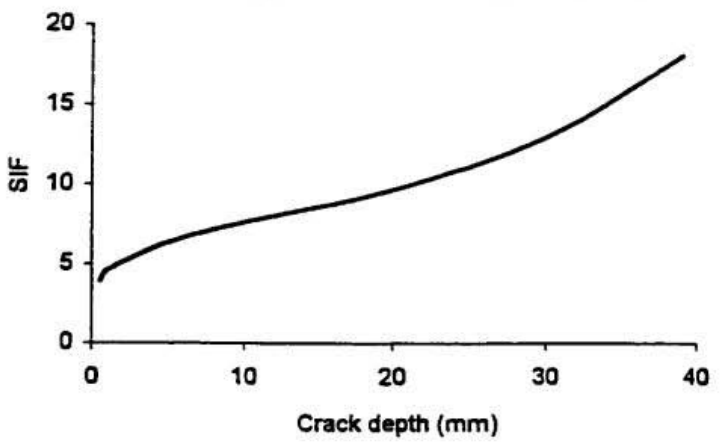

Figure 5.21 Stress intensity factor vs crack depth

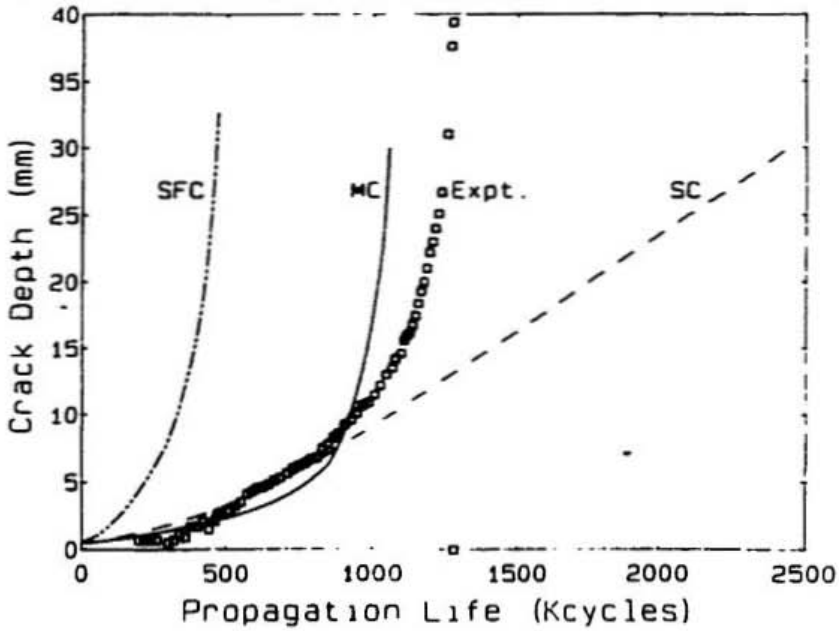

Figure 5.22 Fatigue crack growth (Bell)

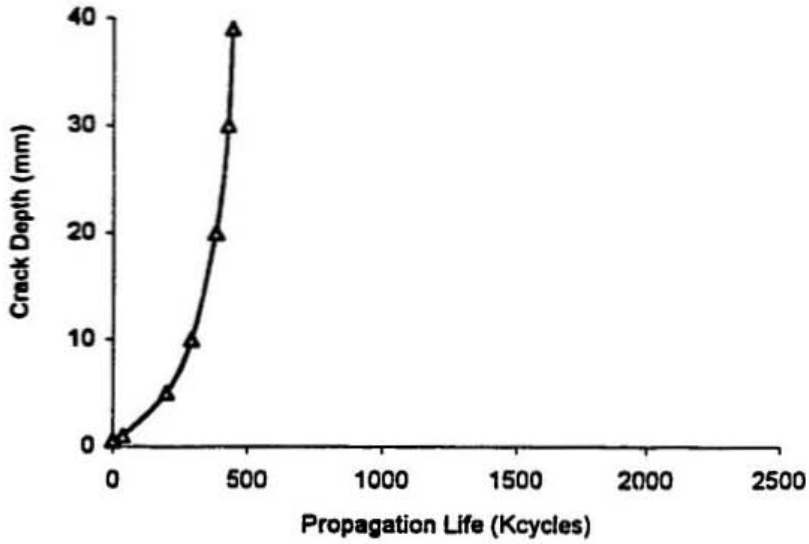

Figure 5.23 Fatigue crack growth using EH-elements

Discussions

1. The stress intensity factors are obtained by using coarse meshes of 20-25 elements. However to have regular sized elements for small crack depths of 0.5 mm and 1.0 mm, a slightly refined mesh of 38 elements is used.

2. The fatigue crack growth curve obtained from Paris crack propagation equation has quite the expected profile and is similar to that given by Bell for a straight fronted crack. The fatigue life of 442 Kcycles obtained in this study is in close agreement with the value, ~480 Kcycles, obtained from the graph provided by Bell for the same problem. The use of coarse meshes for SIF evaluation is thus also validated by a practical example.

5.5 3D EH-Element

5.5.1 Double edge cracked specimen

This problem is an extension of the 2D case (§5.2.1, Fig. 5.5) having 2D SIF reference value as 2.00. The thickness of the specimen, t, in the third dimension is taken as 2.0 and the meshes analyzed are a simple 4 element and a 24 element mesh shown in Fig. 5.24. The results are presented in Table 5.8 and Table 5.9 for values of K_I, for p varying from one to three and at locations z/t, where $z=0$ at the free surface and $z=0.5t$ at the middle of the crack front.

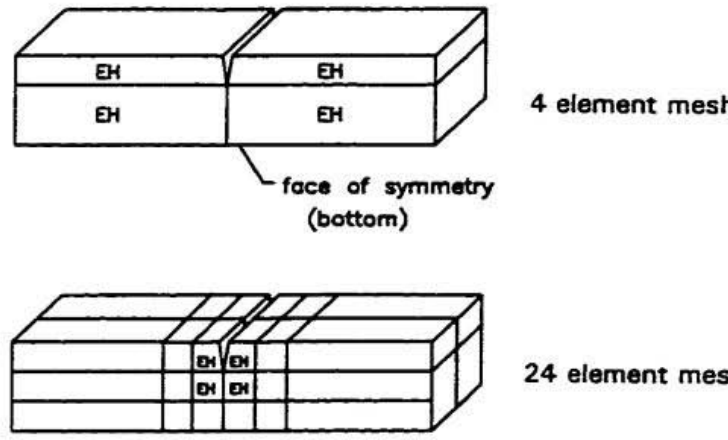

Figure 5.24 Meshes for 3D double edge cracked specimen

Table 5.8 K_I/K_{2D} for double edge cracked specimen, 4 element mesh

	z/t = 0	z/t = 0.5
$p=1$	0.87	0.83
$p=2$	0.84	1.13
$p=3$	0.80	1.10

Table 5.9 K_I/K_{2D} for double edge cracked specimen, 24 element mesh

	z/t = 0	z/t = 0.5
$p=1$	0.87	0.84
$p=2$	0.74	0.78
$p=3$	0.70	0.75

Discussions

1. An average accuracy of 80-90% is achieved in the SIF value for third order coarse meshes of 4 and 24 elements. The NDOF involved are only 257 and 959 respectively

2. The refinement of the mesh, however, does not seem to influence the overall result.

5.5.2 Compact tension fracture specimen

The specimen selected is a plate with through-thickness edge crack of depth a with thickness, half-width and half-height taken equal to a. A uniformly distributed force of P/unit length through the thickness is applied at the crack ends and normal to them. The geometry of this problem, also solved by Tracey [16], is illustrated in Fig. 5.25. The Poisson's ratio is taken as 0.3. The reference solution is taken as a 2D SIF value given by $K_{2D} = 7.20\ P\ a^{-½}$. The meshes used for the analysis are simple 4 element and 32 element meshes given in Fig. 5.26. Table 5.10 and Table 5.11 give the values of K/K_{2D}

along the crack front where $z/a=0$ is the free surface and $z/a=0.5$ is the middle of the crack front. From experience in the 2D cases, the symmetry about the crack front is not considered and the crack is modelled as a whole.

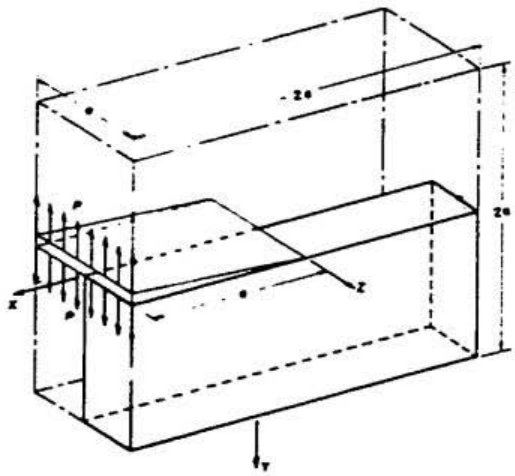

Figure 5.25 Compact tension fracture specimen

Table 5.10 K/K_{2D} for compact tension specimen, 4 element mesh

	z/a = 0	z/a = 0.5
$p=1$	0.76	0.73
$p=2$	0.99	1.08
$p=3$	0.83	0.97

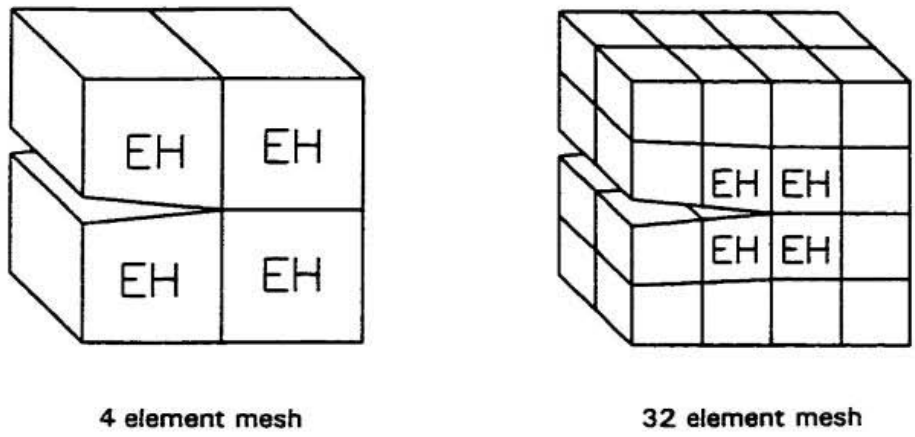

Figure 5.26 Meshes for compact tension fracture specimen

Table 5.11 K/K_{2D} for compact tension specimen, 32 element mesh

	z/a = 0	z/a = 0.5
$p=1$	1.02	1.13
$p=2$	0.82	0.99
$p=3$	0.77	0.93

Discussions

1. The average results along the crack front are within 18% of the 2D reference value for both the meshes. Again the mesh refinement does not influence the overall result.

2. Tracey used a 522 element (660 node, about 2000 DOF) mesh to solve this

problem. Tracey has noted from literature an expected elevation of results by 10% at z/a=0.5 and lower K equal to $0.72K_{2D}$ at the free surface. He obtained results within 1% of K_{2D} at z/a=0.5, and at the free surface the results obtained are $0.79K_{2D}$ and $0.67K_{2D}$ from displacement and stress data respectively.

3. The 4 and 32 element meshes (Fig. 5.26), with p_{max}=3, involve 273 and 1317 DOF respectively. The results at the mid point of crack front are within 3% and 7% of K_{2D} and at the free surface are $0.83K_{2D}$ and $0.77K_{2D}$ for the 4 and 32 element meshes respectively. The additional advantage observed is the ease in construction of meshes using P- and EH-elements.

5.5.3 Semi-circular surface crack in a plate

A plate with a semi-circular surface crack subjected to tension is analyzed for stress intensity factors. The geometry of the problem is shown in Fig. 5.27. The Poisson's ratio is taken as 0.3. The dimensions of the model selected are such that $b/a = h/a = 5$. Two a/t ratios of 0.2 and 0.8 are selected and the meshes constructed using 3D P-and EH-elements are shown in Fig. 5.28. Symmetry of the crack is taken into account and half the specimen is modelled. Fig. 5.28 depicts the meshes (of 13 and 16 elements) for one quarter of the specimen on one side of the crack plane, the other side is similarly modelled (to give a total of 26 and 32 elements). The SIF are evaluated along the crack front from the free surface (ϕ=0°) to the deepest interior point (ϕ=90°). The results are compared with those given by Raju and Newman [24] and are presented in Fig. 5.29 as a ratio of results obtained via MUNSID (K_{EH}) to the reference results (K_{Ref}).

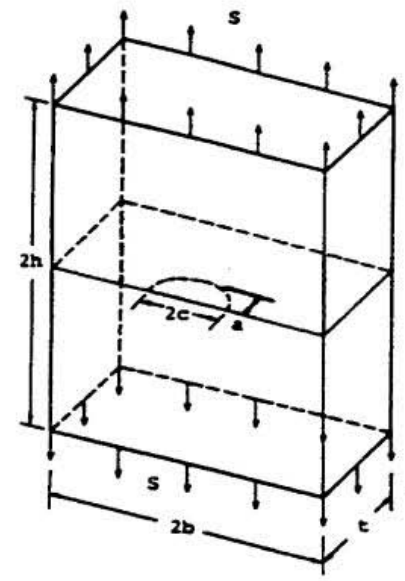

Figure 5.27 Semi-circular crack in a plate

Discussions

1. The results obtained for *a/t* ratios of 0.8 and 0.2 are within 10% and 13% of the reference values respectively. The results are obtained for a maximum order of three. The NDOF involved for the two analyses are 1072 and 1161 compared to refined 6000 DOF models used in [24].

2. The significance of the results obtained in this study is highlighted by the decrease in the NDOF involved by as much as 80%. As regards the error, [24] has noted for 3D semi-elliptical crack analyses, the closest result obtained in the literature as 10-25% lower and a disagreement of 50-100% in the results among some of the authors. The results obtained using EH-elements, within 13% of the reference values ([24]), are thus in good agreement.

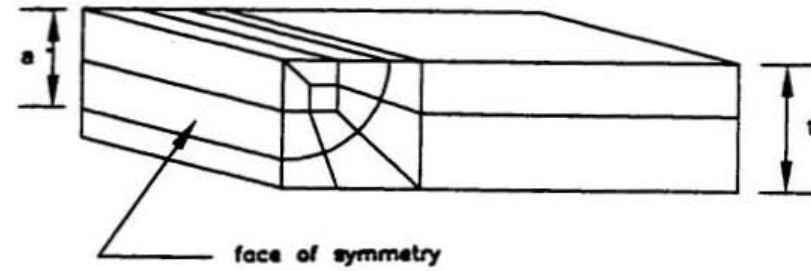

a/t=0.8 26 element mesh

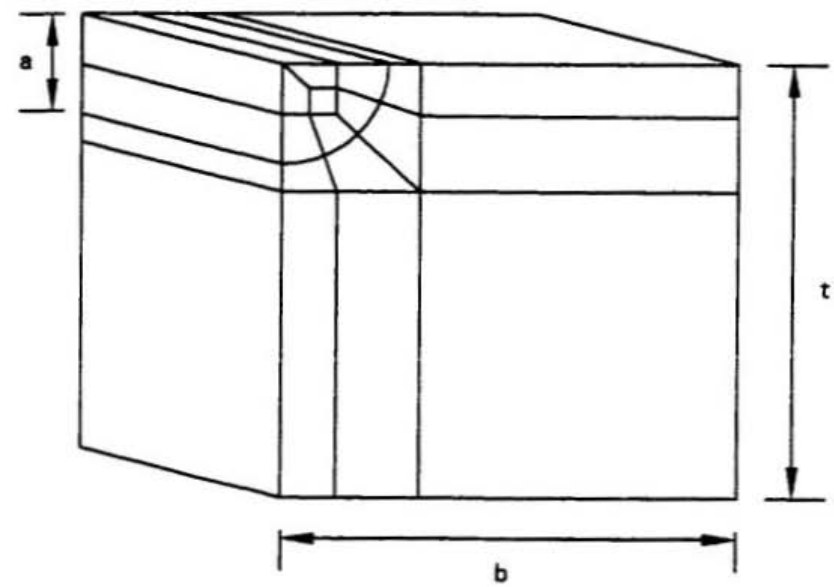

a/t=0.2 32 element mesh

Figure 5.28 Meshes for semi-circular crack

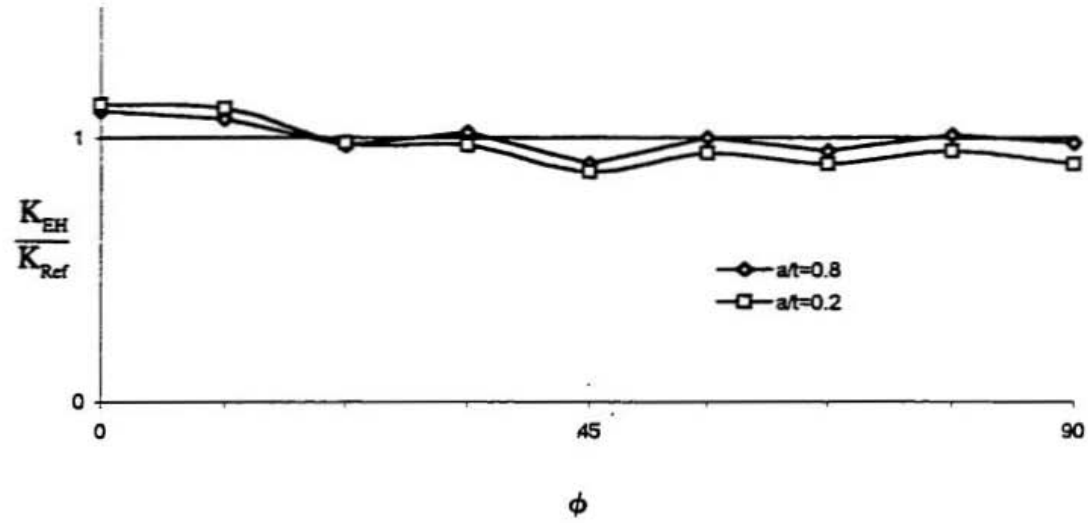

Figure 5.29 SIF results along the crack front

Chapter VI

CONCLUSIONS AND RECOMMENDATIONS

6.1 Conclusions

A practical insight of *p*-version FEM is obtained in this study for plane elasticity problems. An effective 2D Enriched Hierarchical element for LEFM problems is developed and is extended to 3D crack problems. The conclusions of the study presented in the following sections are for the coarsest meshes with reasonable numerical accuracy in comparison with reference values. Higher degree of numerical accuracy is and can be achieved with refined meshes. This study has shown the use of coarse meshes (with large aspect ratio elements) for stress concentration and stress singularity problems that eliminates a large amount of user and computer time for mesh generation and refinement. More importantly, there is a sizable reduction in the number of degrees of freedom involved for a significantly accurate analysis. Due to the complex nature of three dimensional problems, especially involving cracks, further investigations of the application of the EH-element vis-a-vis mesh design are required.

6.1.1 P-elements

1. Cantilever beam

A third order 4x1 mesh for the 2D problem gives an error of only 1% in displacement and 0.2% in stress and is thus sufficient for the analysis. The results for the 3D problem are comparable to the 2D problem and hence are not presented.

2. Cook's membrane

The 2D results, using a third order 4x4 mesh, compared with the reference values have an accuracy of greater than 99% for both displacements and stresses. The results for the 3D problem are again comparable to the 2D problem and are not presented.

3. T-plate welded joint

The SCF and stress profiles through base plate thickness at the weld toe obtained for 45° and AWS weld profiles with t/T ratios of 1.0 and 0.75 are in close proximity to those obtained by Bell. The results obtained are for very coarse meshes (maximum 22 elements) including large aspect ratio elements and a maximum order of six. There is a substantial reduction in the number of degrees of freedom involved compared with those in *h*-version FE analyses.

6.1.2 EH-elements

1. Double edge cracked specimen

The 2D results obtained from fifth order meshes of 4 to 18 elements with 4 EH-elements centred at the crack tip are within $\pm 5\%$ of the reference solution. The elements in the 4 element mesh have an aspect ratio of 1:10. The results obtained for the 3D specimen

have an accuracy of an average of 85% for coarse 4 element and a 24 element meshes. The accuracy of the results has significant importance when compared to the large number of degrees of freedom normally involved in standard 3D analyses.

2. Slant cracked tensile specimen

A third order 18 element mesh with four 2D EH-elements centred at the crack tip gives an error of less than 2.2% for K_I and K_{II} which is quite accurate for the mixed mode SIF problem considered.

3. 45° weld profile T-plate

The T-plate joint selected for analysis has t=78 mm with a t/T ratio of 1.0. The SIF solution is obtained for varying crack depths at the weld toe with coarse 20 to 38 element meshes and a maximum order of five. The fatigue life of 442 Kcycles estimated from the SIF results is compared to that given by Bell and has an accuracy of 90%.

4. 3D compact tension specimen

The values of the SIF obtained from third order 4 element and 32 element meshes are compared to the 2D reference value and have an average accuracy of 88% and 96% respectively. The decrease in the number of degrees of freedom is about 25% compared to the *h*-version analysis in literature. The additional advantage is the relative ease in the construction of the meshes.

5. 3D semi-circular surface crack in a plate

For the two *a/t* crack ratios analyzed using EH-elements, the results are within 13% of the reference values. This close agreement of the results is obtained utilizing only one-fifth the number of degrees of freedom involved in the analyses for the reference values. The relative ease in the construction of meshes using P- and EH-elements is very

significant as an enormous amount of time is usually spent by the human user to prepare the meshes (in *h*-version) for such analyses.

6.2 Recommendations

1. Internal nodes

This work was undertaken considering no internal shape functions for the hierarchical elements. The results obtained show that it had no effect on the solution of the problems analyzed, however, the inclusion of internal nodes especially for shell and plate problems involving bending is recommended. In that case the elemental stiffness matrix is to be assembled into the global matrix after static condensation.

2. Smoothing function

For the EH-element used to determine stress intensity factors in problems involving cracks, the non-conformal formulation is used that employs no zeroing function in the EH-element for compatibility with adjacent P-elements. This had no significant effect on the results obtained, however various zeroing functions can be tested and a suitable one can be included in the formulation to further enhance the accuracy.

3. Error estimation and adaptive schemes

Mesh design using P-elements does not play a critical role in the final results, however optimal results can be achieved by employing a proper balance between *h*-refinement and *p*-refinement. The hierarchical formulation also affords an ease in error estimation that combined with *p*-refinement can provide efficient adaptive solution strategies.

REFERENCES

[1] O.C. Zienkiewicz and R.L. Taylor, *The Finite Element Method*, Vol I, McGraw-Hill, UK (1989).

[2] B. Irons, *Techniques of Finite Elements*, Halsted Press, NY (1980).

[3] K.J. Bathe, *Finite Element Procedures in Engineering Analysis*, Prentice-Hall, NJ (1982).

[4] A. Peano, "Hierarchies of conforming finite elements for plane elasticity and plate bending", *Comp. & Maths. with Appls.*, 2, 211-224 (1976).

[5] M.P. Rossow and I.N. Katz, "Hierarchical finite elements and precomputed arrays", *Int. J. Num. Methods Eng.*, 12, 977-999 (1978).

[6] I. Babuska, B.A. Szabo and I.N. Katz, "The p-version of the finite element method", *SIAM J. Num. Anal.*, 18, 515-544 (1981).

[7] O.C. Zienkiewicz, J.P. de S.R. Gago and D.W. Kelly, "The hierarchical concept in finite element analysis", *Comp. & Struc.*, 16, 53-65 (1983).

[8] B.A. Szabo, "Mesh design for the p-version of the finite element method", *Comp. Methods Appl. Mech. Eng.*, 55, 181-197 (1986).

[9] I. Babuska, "The p and h-p versions of the finite element method: The state of the art", In *Finite Elements: Theory and Applications* (Ed. D.L. Dowyer et al), 199-239 (1988).

[10] N. Wiberg and P. Moller, "Formulation and solution of hierarchical finite element equations", *Int. J. Num. Methods Eng.*, 26, 1213-1233 (1988).

[11] I. Babuska, M. Griebel and J. Pitkaranta, "The problem of selecting the shape functions for a p-type finite element", *Int. J. Num. Methods Eng.*, 28, 1891-1908 (1989).

[12] R.B. Morris, Y. Tsuji and P. Carnevali, "Adaptive solution strategy for solving large systems of p-type finite element equations", *Int. J. Num. Methods Eng.*, 33, 2059-2071 (1992).

[13] S.K. Chan, I.S. Tuba and W.K. Wilson, "On the finite element method in linear fracture mechanics", *Eng. Frac. Mech.*, 2, 1-17 (1970).

[14] J.R. Rice, "A path independent integral and the approximate analysis of strain concentration by notches and cracks", *Trans. A.S.M.E.J. Appl. Mech.*, **35**, 379 (1968)

[15] D.M. Tracey, "Finite elements for determination of crack tip elastic stress intensity factors", *Eng. Frac. Mech.*, 3, 255-265 (1971).

[16] D. M. Tracey, "Finite elements for three-dimensional elastic crack analysis", *Nuclear Eng. Des.*, 26, 282-290 (1974).

[17] T.K. Hellen, "On the method of virtual crack extensions", *Int. J. Num. methods Eng.*, 9, 187-207 (1975).

[18] R.D. Henshell and K.G. Shaw, "Crack tip finite elements are unnecessary", *Int. J. Num. Methods Eng.*, 9, 495-507 (1975).

[19] R.S. Barsoum, "On the use of isoparametric finite elements in linear fracture mechanics", *Int. J. Num. Methods Eng.*, 10, 25-37 (1976).

[20] W.S. Blackburn, "Calculation of stress intensity factors at crack tips using special finite elements", *Conf. Maths. of Finite Elements and Applications*, Brunel Univ., 327 (April 1972).

[21] W.S. Blackburn and T.K. Hellen, "Calculation of stress intensity factors in three dimensions by finite element methods", *Int. J. Num. methods Eng.*, 11, 211-229 (1977).

[22] S.E. Benzley, "Representation of singularities with isoparametric finite elements", *Int. J. Num. Methods Eng.*, 8, 537-545 (1974).

[23] L.N. Gifford, Jr. and P.D. Hilton, "Stress intensity factors by enriched finite elements", *Eng. Frac. Mech.*, 10, 485-496 (1978).

[24] I.S. Raju and J.C. Newman, Jr., "Stress-intensity factors for a wide range of semi-elliptical surface cracks in finite-thickness plates", *Eng. Frac. Mech.*, 11, 817-829 (1979).

[25] G.R. Heppler and J.S. Hansen, "A high accuracy finite element analysis of cracked rectilinear anisotropic structures subject to biaxial stress", *Num. Methods Frac. Mech.*, 223-237 (1980).

[26] R. Bell, "Determination of stress concentration factors and stress intensity factors

for various weld and joint geometries", Final report on D.S.S. Contract 15SQ.2340-4-9276/02 Corrosion Fatigue, Phase III, Carleton Univ./KEJ Engineering, Ottawa, (1990)

[27] G.C. Sih and H. Liebowitz, Mathematical theories of brittle fracture. In *Fracture* (Ed. H. Liebowitz), 11, 67-190, Academic Press, New York (1968).

[28] D.J. Allman, "A quadrilateral finite element including vertex rotations for plane elasticity problems", *Int. J. Num. Methods Eng.*, **26**, 717-739 (1988).

[29] P.G. Bergan and C.A. Fellipa, "A triangular membrane element with rotational degrees of freedom", *Comp. Methods Appl. Mech.*, 50, 25-60 (1985).

[30] R.H. MacNeal and R.L. Harder, "A refined four-noded membrane element with rotational degrees of freedom", *Comp. Struct.*, **18**, 75-84 (1988).

[31] A. Ibrahimbegovic, R.L. Taylor and E.L. Wilson, "A robust quadrilateral membrane finite element with drilling degrees of freedom", *Int. J. Num. Methods Eng.*, **30**, 445-457 (1990).

[32] S. Timoshenko and J.N. Goodier, *Theory of Elasticity*, McGraw-Hill, New York, 1951.

[33] R.D. Cook, "Improved two-dimensional finite element", *J. Struct. Div. ASCE*, **100**, 1851-1865 (1974).

[34] W.F. Brown, Jr. and J.E. Strawley, *Plane Strain Crack Toughness Testing if High Strength Metallic Materials, ASTM Spec. Tech. Publ.*, 410 (1966).

[35] O.L. Bowie, Solutions of plane crack problems by mapping techniques, In *Mechanics of Fracture*. (Ed. G.C. Sih), 1, 1-66, Noordhoff, Leyden (1973).

[36] A. Bignonnet, Y. Papaddopoulos, F. Barrere, H.P. Lieurade and H. Lecoq, "The influence of cathodic protection and post weld improvement on the fatigue resistance of steel welded joints", *Steel In Marine Structures* (Ed. C. Noordhoek and J. de Back), 737-746 (1987).

[37] X. Niu and G. Glinka, "The Weld Profile Effect On Stress Intensity Factors in Weldments", *Int. J. Fracture*, 35, 3-20 (1987).

APPENDIX A

Shape functions for a 2nd order 3D P-element

$$N_i^1 = \frac{1}{8}(1+\xi_i\xi)(1+\eta_i\eta)(1+\zeta_i\zeta)\left(\frac{l_i}{2}\right)^2 \qquad i = 1 \text{ to } 8$$

$$N_i^2 = \frac{1}{8}(\xi^2-1)(1+\eta_i\eta)(1+\zeta_i\zeta)\left(\frac{l_i}{2}\right)^2 \qquad i = 9, 11, 17, 19$$

$$N_i^2 = \frac{1}{8}(1+\xi_i\xi)(\eta^2-1)(1+\zeta_i\zeta)\left(\frac{l_i}{2}\right)^2 \qquad i = 10, 12, 18, 20$$

$$N_i^2 = \frac{1}{8}(1+\xi_i\xi)(1+\eta_i\eta)(\zeta^2-1)\left(\frac{l_i}{2}\right)^2 \qquad i = 13, 14, 15, 16$$